Justus-Liebig-Universität Gießen
I. Physikalisches Institut

Charge-Carrier Recombination in Dilute Bismuthide Semiconductors

Dissertation
zur Erlangung des Doktorgrades der Naturwissenschaften

- Dr. rer. nat. -

dem Fachbereich 07
Mathematik und Informatik, Physik, Geographie
vorgelegt von

Julian Veletas

Gießen, März 2021

Erstgutachter: Prof. Dr. Sangam Chatterjee
Zweitgutachter: Prof. Dr. Kerstin Volz

EIGENSTÄNDIGKEITSERKLÄRUNG

Ich erkläre:
Ich habe die vorgelegte Dissertation selbstständig und ohne unerlaubte fremde Hilfe und nur mit den Hilfen angefertigt, die ich in der Dissertation angegeben habe. Alle Textstellen, die wörtlich oder sinngemäß aus veröffentlichten Schriften entnommen sind, und alle Angaben, die auf mündlichen Auskünften beruhen, sind als solche kentlich gemacht. Ich stimme einer eventuellen Überprüfung meiner Dissertation durch eine Antiplagiat-Software zu. Bei den von mir durchgeführten und in der Dissertation erwähnten Untersuchungen habe ich die Grundsätze guter wissenschaftlicher Praxis, wie sie in der „Satzung der Justus-Liebig-Universität Gießen zur Sicherung guter wissenschaftlicher Praxis“ niedergelegt sind, eingehalten.

_____ Gießen, 03.03.2021

(Julian Veletas)

KURZFASSUNG

Die stark zunehmende Internetnutzung durch Cloud-Services oder Streaming basierte Anwendungen erzeugt eine stetig wachsende Nachfrage an schneller und stabiler Datenübertragung. Halbleiterlaser bilden derzeit einen der zentralen Bestandteile der dafür benötigten Datenkommunikationsinfrastruktur. Aufgrund der anspruchsvollen Fertigung und der relativ niedrigen Energieeffizienz dieser Laser ist es Ziel aktueller Forschung, neue Materialsysteme oder Konzepte zu untersuchen. Hier sind in den vergangenen Jahren bismuthaltige Halbleitersysteme in den Fokus der angewandten Halbleiterforschung gerückt. Sie versprechen neben einer höheren Energieffizienz auch eine hohe Bandbreite an adressierbaren Emissionswellenlängen, die über das Datenübertragungsfenster hinaus in den mittelinfraroten Spektralbereich reichen.
In dieser Arbeit wurde mit spektroskopischen Methoden an zwei Konzepten bismuthaltiger Halbleiter geforscht. Zum einen wurden Ga(N,As)/ Ga(As,Bi) Heterostrukturen untersucht. Hier wird der räumlich indirekte Übergang (Typ-II Übergang) zwischen Elektronen aus den Ga(N,As)-Schichten und Löchern der Ga(As,Bi)-Schichten analyisiert. Ziel war es zu verstehen, wie sich die jeweiligen Schichtfolgen auf die Emissionseigenschaften des räumlich indirekten Übergangs auswirken. Es konnte gezeigt werden, dass die Unordnungseffekte der Ga(N,As)-Schicht maßgeblich die Unordnungscharakteristika der Übergangsenergie beeinflusst, wohingegen die Ga(As,Bi)-Schicht sehr deutlich die Linienbreite dominiert. Als Ursache hierfür konnten lokalisierte Zustände in der Ga(As,Bi)-Schicht identifiziert werden. Des Weiteren wurde der Unterschied zwischen symmetrischen (W) und asymmetrischen Typ-II Strukturen untersucht. Hier zeigt sich, dass die symmetrische Struktur, bestehend aus zwei Ga(N,As)-Schichten, die um die Ga(As,Bi)-Schicht angeordnet sind, geringere Unordnungseffekte

in der Rekombination über den Typ-II Übergang aufweist. Abschließend konnten weitere Experimente Aufschluss über die Rekombinationskanäle in solchen Typ-II und W-Halbleiterstrukturen liefern. So zeigt sich, dass maßgeblich Elektronen, die in den GaAs- und Ga(N,As)-Schichten angeregt werden, zur Rekombination über den räumlich indirekten Übergang beitragen.
Die hier erlangten Ergebnisse geben direkte Informationen über die wichtigsten optischen Verlustkanäle innerhalb der Strukturen und zeigen somit Anhaltspunkte für Optimierungen auf. Somit lässt sich ein zielgerichteter Optimierungsprozess etablieren, der es erlaubt, die optischen Eigenschaften möglichst genau auf ein Anforderungsprofil zuzuschneiden.

Als Zweites wurde das quarternäre Materialsystem (Ga,In)(As,Bi) untersucht. Für Optoelektronik auf der InP-Plattform hat dieses Materialsystem vielversprechende Eigenschaften, um den mittelinfraroten Spektralbereich zu adressieren. Das epitaktische Wachstum dieses quaternären Systems ist herausfordernd, da Bismut den Einbau der Gruppe-III Elemente stark beeinflusst. Somit ist das Abscheiden von Schichten mit spezifischer Komposition erschwert. Durch Photolumineszenz- und Röntgenphotoelektronenspektroskopie konnte ein Zusammenhang zwischen Unordnungseigenschaften und Wachstumsparametern hergestellt werden. Gallium- und Bismutpräkursorpartialdrücke während des Wachstums konnten mit der Bismutsegregation korreliert werden. Dadurch kann eine verbesserte Wachstumskontrolle ermöglicht werden. Die Untersuchung der Ladungsträgertemperaturen mittels Photolumineszenzspektroskopie ergab, dass diese ebenfalls durch die Präkursorgenpartialdrücke beeinflusst sind. Für niedrigere Galliumpartialdrücke konnten niedrigere Ladungsträgertemperaturen und somit geringere Unordnungseffekte beobachtet werden.

ABSTRACT

The rapidly increasing use of the internet through cloud services or streaming-based applications creates a steadily growing demand for faster and more stable data transmission. Semiconductor lasers are a key component of the current data communication infrastructure. The aim of current research is to investigate new material systems or concepts to improve the efficiency and reliability of these lasers. In recent years, bismuth containing semiconductors have come into focus. In addition to higher energy efficiency, they also promise to extend the range of addressable emission wavelengths beyond the data-communication band into the mid-infrared spectral range.

In this thesis, two concepts of bismuth containing semiconductors are analyzed using spectroscopic methods. On the one hand, Ga(N,As)/ Ga(As,Bi) heterostructures are investigated. Here, the spatially indirect transition (type-II transition) between electrons from the Ga(N,As) layers and holes in the Ga(As,Bi) layers is analyzed. The aim is to understand, how the respective layers affect the emission properties of the spatially indirect transition. The disorder effects of the Ga(N,As) layers significantly influence the disorder characteristics of the emission energy, whereas the Ga(As,Bi) layer clearly dominates the line width. Localized states in the Ga(As,Bi) layer are identified as the cause. Furthermore, the difference between symmetric (W) and asymmetric type-II structures is investigated. The symmetric structure consists of two Ga(N,As) layers, which are arranged around the Ga(As,Bi) layer. Fewer disorder effects in the recombination via the type-II transition are observed for the symmetric arrangement. Finally, additional experiments provide information about the recombination channels in such type-II and W-type semiconductor heterostructures. Electrons that are excited in the GaAs and Ga(N,As) layers contribute significantly to the recombination via the

spatially indirect transition.
The results obtained here provide direct information about the dominant optical loss channels within the structures and, thus, point to potentials for optimization. This enables targeted improvements that allow the optical properties to be tailored as precisely as possible to a requirement profile.

Secondly, the quaternary material system (Ga,In)(As,Bi) is investigated. For optoelectronics on the InP platform, this material system has very promising properties for addressing the mid-infrared spectral range. The epitaxial growth of such quaternary system is challenging. In particular, as bismuth has a strong influence on the incorporation of the Group-III elements. This makes it difficult to deposit layers with a specific desired elemental composition. Using input from photoluminescence and X-ray photoelectron spectroscopy, establishes a relation between disorder properties and growth parameters. Gallium and bismuth precursor partial-pressures during growth are correlated with bismuth segregation. This enables improved growth control. The investigation of the charge-carrier temperatures by means of photoluminescence spectroscopy shows that they are influenced by the precursor partial-pressures, too. For lower gallium partial pressures, lower charge-carrier temperatures and, thus, lower disorder effects are observed.

AUTHOR'S CONTRIBUTIONS

Parts of the scientific findings established during my dissertation are currently published in peer-reviewed journals. These can be seen as milestones of my dissertation and represent the major scientific advances. In addition, the work presented here has been frequently presented and discussed on international conferences and workshops to share the results with the scientific community. In this way, new concepts and stimuli are gathered and implemented.

Publications in peer-reviewed journals

[1] J. Veletas et al. "Comparison of Carrier-Recombination in Ga(As,Bi)/ Ga(N,As) - Type-II Quantum Wells and W-type Heterostructures". In: *Appl. Phys. Lett.* 118 (2021), p. 052103.

[2] J. Veletas et al. "Bismuth surface segregation and disorder analysis of quaternary (Ga,In)(As,Bi)/InP alloys". In: *J. Appl. Phys.* 126 (2019), p. 135705.

Conference contributions

[1] J. Veletas et al. "Ga(As,Bi)-based W-Type Alloys". In: *GRK 1782 Workshop*. Poster, Schwäbisch Gmünd, Germany, Sept. 2019.

[2] J. Veletas et al. “Surface Diffusion and Disorder in Quaternary (Ga,In)/ (As,Bi)/ InP Heterostructures”. In: *10th International Workshop on Bismuth-Containing Semiconductors*. Contributed talk, Toulouse, France, July 2019.

[3] J. Veletas et al. “XPS and Disorder Analysis of Quaternary (Ga,In)(As,Bi) Semiconductor Alloys”. In: *DPG Frühjahrstagung*. Contributed talk, Regensburg, Germany, Mar. 2019.

[4] J. Veletas et al. “Influence of Bi Incorporation in Quaternary Alloys”. In: *2nd Joint Seminar GRK 1782 and SFB 1083*. Contributed talk, Volkenroda, Germany, Sept. 2018.

[5] J. Veletas et al. “Influence of Bi Incorporation in Quaternary Alloys”. In: *9th International Workshop on Bismuth-Containing Semiconductors*. Contributed talk, Kyoto, Japan, July 2018.

[6] J. Veletas et al. “Emission and Disorder Properties of Quaternary (Ga,In)(As,Bi) Semiconductor Alloys”. In: *DPG Frühjahrstagung*. Poster, Berlin, Germany, Mar. 2017.

[7] J. Veletas et al. “Optical Characterization of Quaternary (Ga,In)(As,Bi Semiconductor Alloys)”. In: *8th International Workshop on Bismuth-Containing Semiconductors*. Poster, Marburg, Germany, July 2017.

[8] J. Veletas et al. “Optical Spectroscopy on Dilute Bismuthide Semiconductors”. In: *Materialforschungstag Mittelhessen*. Poster, Giessen, Germany, June 2017.

[9] J. Veletas et al. “Optical Characterization of Quaternary GaInAsBi Semiconductor Alloys”. In: *DPG Frühjahrstagung*. Contributed talk, Dresden, Germany, Mar. 2017.

CONTENTS

LIST OF FIGURES

ABBREVIATIONS

IR	infrared
Bi	bismuth
SO	split-off
Ga(As,Bi)	gallium arsenide bismuthide
(Ga,In)(As,Bi)	gallium indium arsenide bismuthide
GaAs	gallium arsenide
InP	indium phosphide
Ga(N,As)	gallium nitride arsenide
QW	quantum well
BAC	band anti-crossing
VCA	virtual crystal approximation
N	nitrogen
CB	conduction band
VB	valence band
InAs	indium arsenide
PL	photoluminescence
FWHM	full width at half maximum
PLE	photoluminescence excitation
XPS	X-ray photoelectron spectroscopy
FTIR	Fourier-transform infrared
PR	photomodulated reflectance
PT	photomodulated transmittance

CHAPTER 1

INTRODUCTION

Optoelectronic devices are key components in various domains of modern technology. Today's data communications rely on optical signals guided via optical fibers. It is highly desired to use wavelength bands where effects of attenuation and dispersion of the optical signals in fiber-optics are minimized. According to that, the most widely used wavelength bands are the 1.3 µm and 1.55 µm wavelength regions.[1,2] Hence, data communications require lasers emitting in these bands. These infrared (IR) wavelength bands are commonly referred to as telecom bands or telecom windows, the latter referrers to the fiber transmission.

Another application for optoelectronics is sensor technology. Desired sensors operate at longer wavelengths compared to the telecom wavelengths, since, e.g., in medical applications, bio sensing, and environmental sensing, the discrete absorption bands of molecular vibrations are probed.

Overall, the demand for IR optoelectronic devices rises continuously. Nonetheless, state-of-the-art technology devices for IR applications suffer from two major constraints: (1) a lack of efficiency or, (2) the intended emission wavelengths cannot be addressed using current materials. The main loss channel, and, therefore, the highest limitation for the efficiency of an optoelectronic device, are Auger losses.[3] These Auger losses describe processes of nonradiative carrier recombination which result in a heating of the material.[4] Several years ago, it was predicted that some of these loss channels can potentially be suppressed in bismuth containing semiconductors.[5] The incorporation of bismuth (Bi) into the host crystal lattice leads to a rapid decrease of the band gap energy by simultaneously increasing the spin-orbit coupling energy.[6] Auger

losses involving the split-off (SO)-band can be eliminated, if the spin-orbit splitting energy exceeds the band-gap energy. Thus, materials like gallium arsenide bismuthide (Ga(As,Bi)) or gallium indium arsenide bismuthide ((Ga,In)(As,Bi)) are promising for both, more efficient devices and covering a broader spectral range in the IR.[5] Additionally, these dilute bismuthide semiconductors can be integrated onto the well-established gallium arsenide (GaAs) or indium phosphide (InP) platforms.[7,8]
A subsequent step towards the functionalization of those novel materials is the utilization in semiconductor heterostructures to form a spatially indirect transition (type-II transition).[9–12] Here, the wide scope of band gap engineering of dilute bismuthide semiconductors can be combined with other materials, e.g., gallium nitride arsenide (Ga(N,As)), to form lattice matched near-IR emitters on the GaAs platform.[13]

This thesis aims to advance the relevant science in two aspects. Firstly, the aim of this thesis is the investigation of recombination properties in asymmetric and symmetric Ga(N,As)/ Ga(As,Bi) type-II structures. Not only the specific contribution of each quantum well (QW) in the type-II recombination is investigated, but also the fundamental difference between symmetric and asymmetric structures is of major interest. Secondly, the influence of growth parameters on the optical properties is analyzed, since it offers essential information for the optimization of potential devices. By this means, the surfactant effect of bismuth atoms during the growth of III-V semiconductors is related to the optical properties of the quaternary material (Ga,In)(As,Bi).

In the subsequent chapter, the fundamental aspects of highly mismatched semiconductor alloys (HMAS) are detailed. The development and necessity for the band anticrossing (BAC) model illustrated and the impact on the band structure is described. Furthermore, the main characteristics and differences of dilute nitride and dilute bismuthide semiconductors are discussed. The chapter is closed by a detailed description of the influence of localized states on the optical properties. Chapter 3 describes the spectroscopic methods that are used to obtain the data. The work is concluded and an outlook is given in Chapter 4.

CHAPTER 2

HIGHLY MISMATCHED SEMICONDUCTOR ALLOYS

Alloying semiconductors is one of the most versatile methods in modern semiconductor device fabrication. The feasibility of tuning opto-electronic properties of a material not only strongly broadened the scope of devices such as diode lasers but has also led to technical milestones like, e.g., the optimization of multijunction solar cells. Starting point of the development are ternary semiconductor materials, which are alloyed by binary semiconductors, such as GaAs and aluminum arsenide (AlAs). Vegard[14] found, that the lattice constant of the two constituents a_{AB} is a weighted mean of the two components' lattice constant:

$$a_{AB}(x) = x \cdot a_A + (1 - x) \cdot a_B. \tag{2.1}$$

Accordingly, Vurgaftman et al.[15] report on a prediction of the band gap as

$$E_g(x) = x \cdot E_{g,A} + (1 - x) \cdot E_{g,B} + \underbrace{b(x) \cdot x(x - 1)}_{\Delta E_g(x)}. \tag{2.2}$$

Here, $E_{g,A}$ and $E_{g,B}$ are the band gap energies of the respective constituents, while $b(x)$ is the so called bowing factor. The latter is an experimentally estimated value, which accounts for an observed nonlinearity. This interpolation is called virtual crystal approximation (VCA). This versatile approximation can be expanded to quaternary systems by using the ternary lattice parameters and band gaps in Eq. 2.1 and Eq. 2.2,

respectively.
However, the rapid progress in semiconductor growth techniques enables the synthesis of mismatched alloys. E.g., growth under non equilibrium conditions inhibits phase separation and thus, expands the reach of semiconductor devices by far. In an early work in 1992, Weyers et al.[16] report on the large reduction of the band gap of Ga(N,As) by nearly 100 meV per percent nitrogen (N). Similar results are found for the quaternary material gallium indium nitride arsenide ((Ga,In)(N,As)), which pushed the band gap below the 1 eV region and, additionally, can be deposited lattice matched to GaAs.[17] The observed band gap reduction cannot be explained by the VCA. Later findings reveal that not only the band gap is reduced, but the electronic structure of the conduction band at higher energies is modified.[18,19] The interaction between highly localized states of the N atoms in the GaAs matrix forms isovalent defects. The BAC model is then developed to describe the influence of these isovalent impurity levels on the band structure.

2.1 Band Anti-Crossing

Due to the broad range of the electronegativity of the group-V elements (e.g., 3.04, 2.18, and 2.02 in Pauling scale for N, As, and Bi, according to IUPAC standards[20]), substituting small amounts of N or Bi into the GaAs matrix forms isoelectronic traps. The high electronegativity and small covalent radius of N results in a dispersionless impurity band in the conduction band (CB) of the host crystal lattice, while the less electronegative but large Bi atoms with a strong metallic character mainly disturb the valence band (VB) of the host matrix. As an immediate result of the Pauli exclusion principle, an anti-crossing between the original band of the host semiconductor and the impurity related band leads to a splitting and rearrangement of the involved bands (cf. Fig. 2.1 (a)). The Bi related impurity disturbs the VB of the host semiconductor, which is plotted in Fig. 2.1 (b) for the binary systems GaAs and indium arsenide (InAs), relevant for this thesis. The result for both cases is a rapid decrease of the band gap by shifting the CB (VB) towards the Fermi energy with increasing N (Bi) fraction.

In case of the bismuthide alloys, the band gap shrinkage is accompanied by an increase of the spin-orbit coupling energy of the SO band.[7,22–24] The spin-orbit coupling

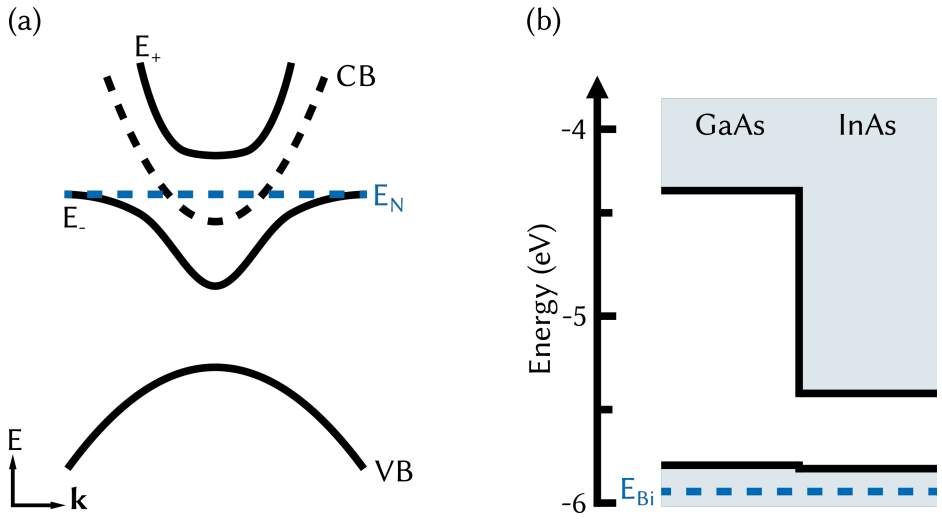

Fig. 2.1: The splitting and reconstruction of the CB as the consequence of the BAC is illustrated in (a) for Ga(N,As) (solid lines). The dashed lines indicate the uncorrelated bands. The Bi induced impurity band energy and the band offsets of GaAs and InAs are shown in (b) (the zero point energy is referenced to gold, according to Ref. [21]).

increases due to the high atomic number of Bi atoms.[25] Therefore, a situation of $E_g < \Delta_{so}$ can be achieved where Auger losses could potentially be suppressed.[26] For light emitting devices, these Auger losses, especially CHSH Auger recombination, are one of the major performance limiting recombination paths.[27] Simulations show, that a Bi fraction of approximately 9%[28] and 4%[29] is sufficient to fulfill this criteria for the ternary alloy Ga(As,Bi) on GaAs and the quaternary alloy (Ga,In)(As,Bi) on InP, respectively. However, recent density functional theory (DFT) studies reveal that the introduction of Bi into the crystal lattice forms new states between the heavy-hole (HH)/ light-hole (LH) and SO band.[30,31] These findings may limit the high increase of device efficiency by suppressing the mentioned Auger losses. Further investigations are necessary to analyze, how those states influence the carrier recombination and how large their oscillator strength is. Nonetheless, this does not affect the wide scope of band gap engineering nor the access to long-wavelength optoelectronics on the GaAs or the InP platform.

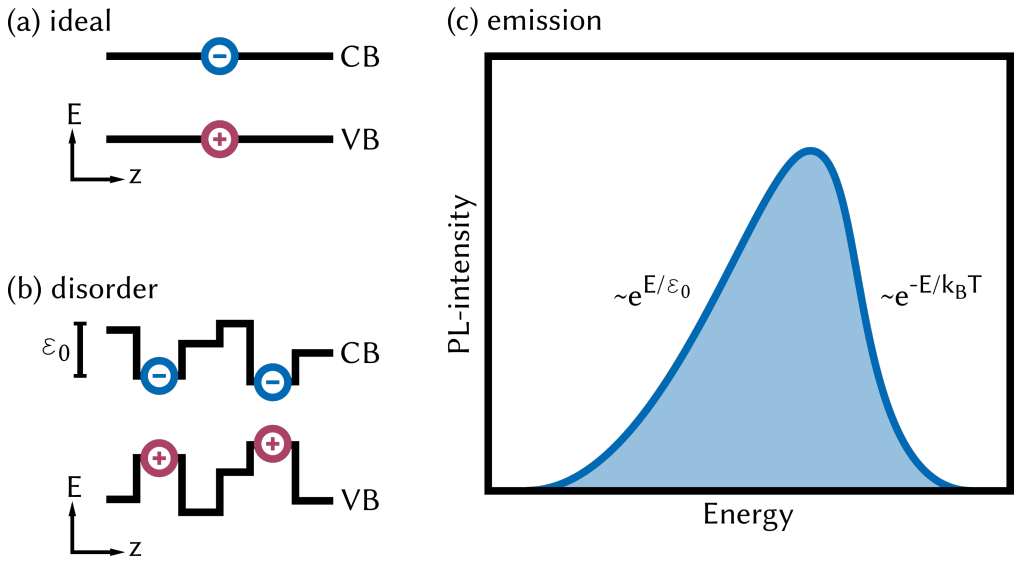

Fig. 2.2: A comparison between the band edges of an ideal semiconductor and a semiconductor with disorder is depicted in (a) and (b), respectively. The resulting influence on the emission properties of such disordered band potential is plotted in (c).

2.2 Disorder and Localized States

The high impact of substituents like N or Bi on the electronic band structure not only extends the accessible range of materials but they intrinsically introduce localized states and disorder in the crystal lattice. The latter can be understood as, e.g., fluctuations in the composition, spatial variations of the widths of QWs or altering internal electric fields. The disordered band edges influence the combined density-of-states (DOS), which then alters the optical response. Figure 2.2 (a) and (b) illustrate the difference between an ideal semiconductor and a disordered semiconductor, respectively. In experiments, the investigated area is way larger than the energy scale ϵ_0 of those potential fluctuations, resulting in inhomogeneous broadening. Additionally, the photoluminescence (PL)-maxima shifts towards lower energies, since the carriers relax into local minima of the disordered band edges. Accordingly, a distinctive PL spectrum of a semiconductor with disorder is pictured in Fig. 2.2 (c).

The PL-spectrum can be divided into two spectral regions: (i) the low-energy flank, which is dominated by the distribution of the band-tail states and (ii) the high-energy

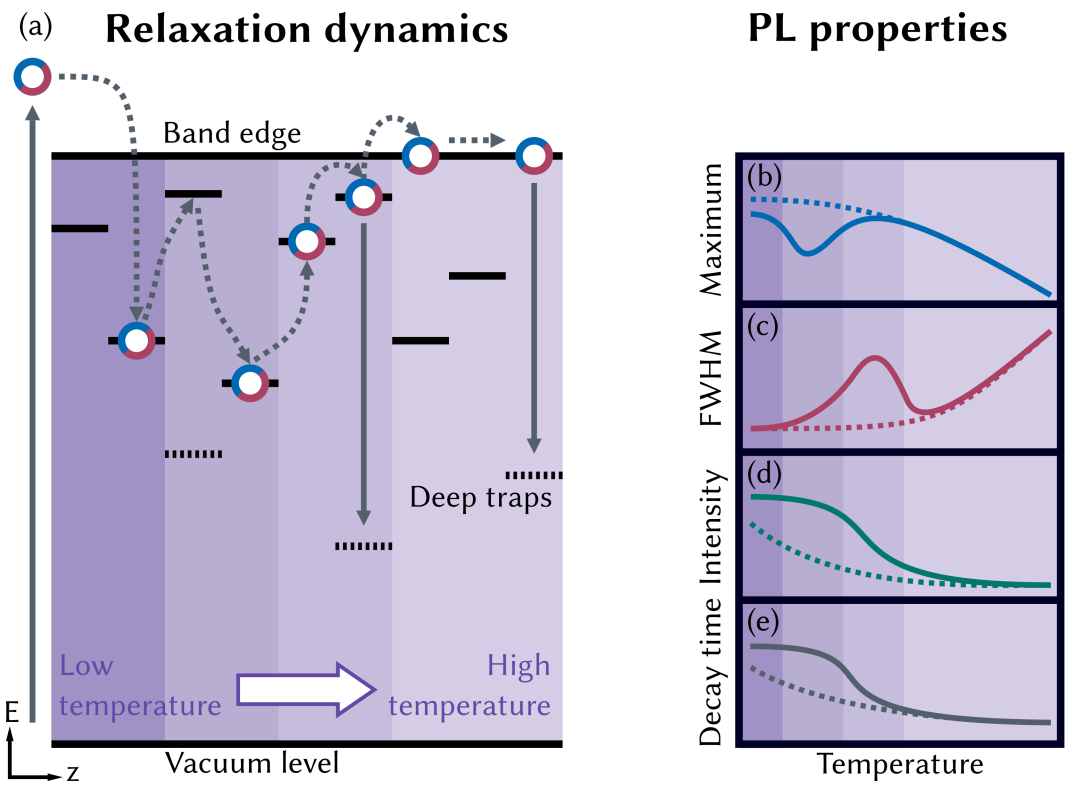

Fig. 2.3: The thermally activated hopping process of excitons is visualized in (a). On the right-hand side, the respective impact on PL-maxima (b), FWHM (c), intensity (d), and decay time (e) are drawn. The dotted lines on the right-hand side correspond to an ideal semiconductor. (Figure based on Chernikov[32])

side, which is dominated by homogeneous broadening and carrier temperatures. These two regimes are energetically separated and thus, they can be treated independently. Carrier temperatures deviate from a pure Boltzmann distribution in the presence of disorder or defect states. Here, transitions to impurity-related bands influence the thermalization process leading to carrier temperatures higher than the crystal lattice temperature.

However, disorder not only influences the line shape of the PL, but has an effect on the temperature dependence of the PL. The temperature dependence of the PL is shown schematically in Fig. 2.3; the carrier-relaxation process is iteratively developed in (a), while (b), (c), (d) and (e) show the influence on the PL-maximum, the full width at half maximum (FWHM), the intensity, and the decay time, respectively. Here, a low excitation density is assumed. Photoexcitation of a semiconductor leads to the

formation of Coulomb-correlated electron-hole pairs (excitons).[33,34] At low temperatures, in a disordered semiconductor these excitons relax via phonon scattering into a localized state. Here, the PL is, thus, shifted to lower energies with respect to the band edge. Additionally, the carrier localization suppresses non-radiative recombination, since the momentum of localized states equals zero and phonon scattering is restricted due to momentum conservation. Thus, PL-intensities are comparatively high. With increasing lattice temperatures, the exciton mobility is increased, too. The excitons are able to leave the local potential minima by phonon-assisted hopping and are able to occupy states at lower energies. This shifts the PL-peak to lower energies. In this temperature regime, the excitons occupy a higher number of localized sites, thus the distribution of possible phonon energies broadens and the FWHM increases. Above a distinct temperature, the exciton distribution approaches thermal equilibrium and occupy higher lying states. The PL-maximum shifts to higher energies and the FWHM reaches a local maximum at $T_2 \approx \epsilon_0/k_B$.[35] The shift of the PL-peak is commonly referred to as *S-shape*.[36] Due to the higher exciton mobility, the probability of exciton capture by deep traps is increased and, thus, the PL-intensity and the decay times decrease. For even higher lattice temperatures, the carriers are thermally activated into delocalized states and the PL properties converging to the band edge PL properties.

Besides the temperature dependence, localized states dominantly affect the excitation density dependence. Figure 2.4 illustrates the impact of the excitation density on the PL of a disordered semiconductor. In (a), two scenarios of different excitation densities are illustrated. The localized states below the band edge capture excited carriers. At low excitation densities and a low lattice temperature, the bound excitons will relax to the local potential minima resulting in a red-shift of the emission energy, as discussed above. However, due to the strong localization of these states, only few bound excitons relax into deep traps. With increasing excitation density, the local potential minima are increasingly filled. Thus, the average energy of the carrier distribution increases leading to a blue-shift of the PL. Simultaneously, the exciton mobility increases because states with higher energies are occupied. Free excitons will form if the exciton mobility reaches the mobility edge. Therefore, the probability of exciton capture by deep traps rises and the intensity increases sublinear.

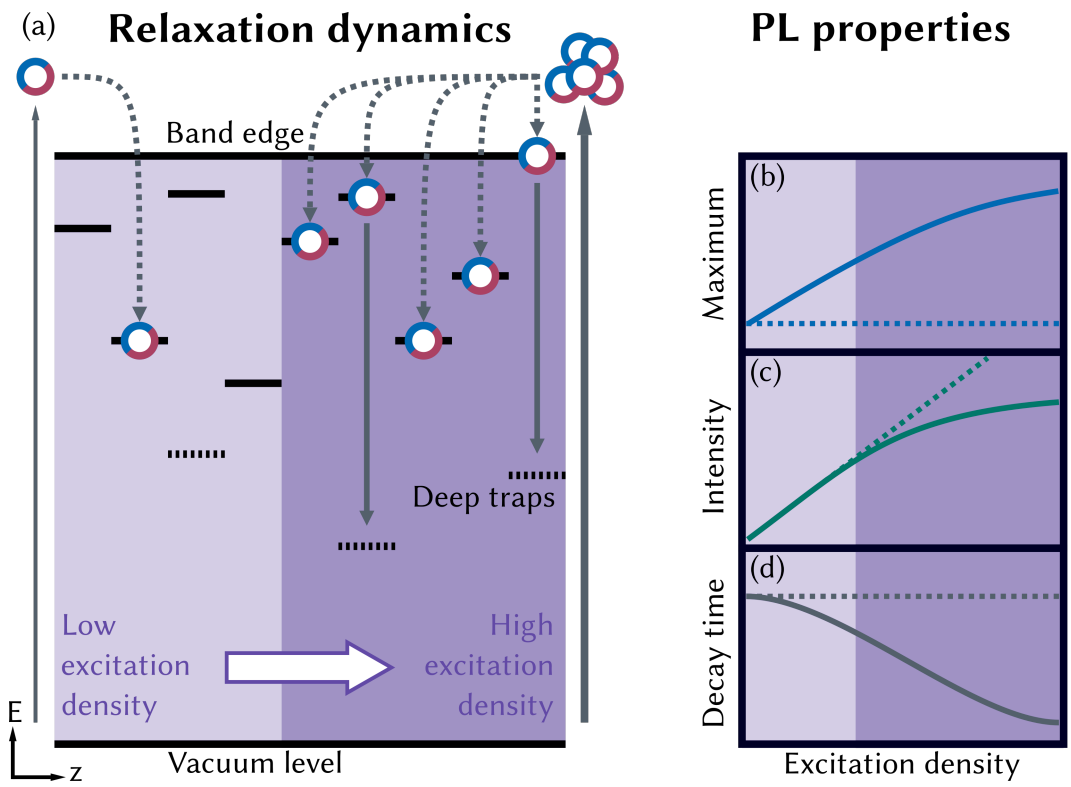

Fig. 2.4: The state-filling process induced by increasing excitation densities is depicted in (a), while (b), (c), and (d) demonstrate the influence on the PL-maxima, PL-intensity, and PL-decay time, respectively. The dotted lines on the right-hand side correspond to an ideal semiconductor. (Figure based on Chernikov[32])

CHAPTER 3

EXPERIMENTALS

This chapter provides an overview of the experimental setups used for the spectroscopic studies. The first section deals with the PL setup as an emissive technique. This is followed by sections describing the absorptive techniques, namely photoluminescence excitation (PLE) spectroscopy and modulation spectroscopy. The fourth section describes the X-ray photoelectron spectroscopy (XPS) setup, which is the only non-optical spectroscopy used here.

3.1 Photoluminescence Spectroscopy

PL measurements are performed using two different experimental setups. A line-scan setup is used for near IR (*NIR*) measurements, while the mid IR (*MIR*) is adressed by Fourier-transform infrared (FTIR) spectroscopy.

The *NIR* setup covers a spectral detection range from 0.73 eV (1700 nm) up to 1.55 eV (800 nm). This experiment is schematically drawn in Fig. 3.1 (PL path, red-shaded area). The samples are mounted in a helium-flow cryostat that enables temperature-dependent measurements from 4 K to 400 K. A diode-pumped continuous-wave intracavity frequency-doubled Nd:YAG laser excites the sample at 2.33 eV (532 nm). The excitation light is mechanically chopped and passes a filter wheel. Here, reflective neutral-density filters enable excitation-density dependent measurements. The excitation light is then focused on the sample leading to a spot size of approximately

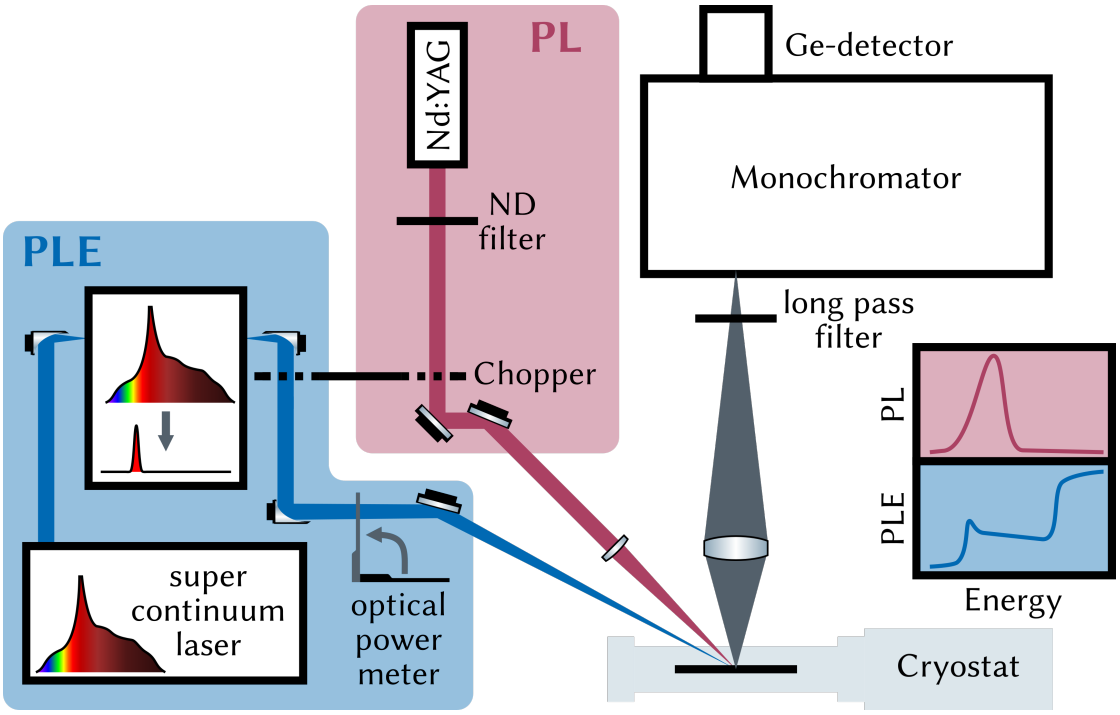

Fig. 3.1: An illustration of the PL (red-shaded area) and the PLE (blue-shaded area) experiments is drawn.

700 µm^2 (estimated from the initial beam diameter and the numerical aperture N_A of the focusing lens). Thus, the excitation density can be tuned from 0.85 W/cm^2 up to a maximum of 11.3 kW/cm^2. The sample's PL is imaged onto the 500 µm entrance slit of a 1 m Czerny-Turner monochromator (grating: 600 g/mm; 1250 nm blaze). This configuration yields a spectral resolution of 1 nm. Phase sensitive line-scan lock-in technique combined with a liquid-nitrogen cooled germanium (Ge) detector quantify the PL signal.

The "MIR" PL experiment (Fig. 3.2) operates within a spectral range of 0.23 eV (5500 nm) and 0.83 eV (1500 nm). Here, the samples are mounted in a closed-cycle helium cryostat. Temperature-dependent measurements from 15 K up to 300 K are possible. For excitation, a 1.91 eV (650 nm) laser diode is focused on the sample leading to an excitation-density of 20 W/cm^2. The PL is collected and collimated by a parabolic mirror and is detected by a liquid-nitrogen cooled indium antimonide (InSb) detector mounted on an FTIR scanner. The FTIR scanner is a Michelson interferometer which measures the interferogram of the luminescence. Using a fast Fourier transform (FFT), the interfer-

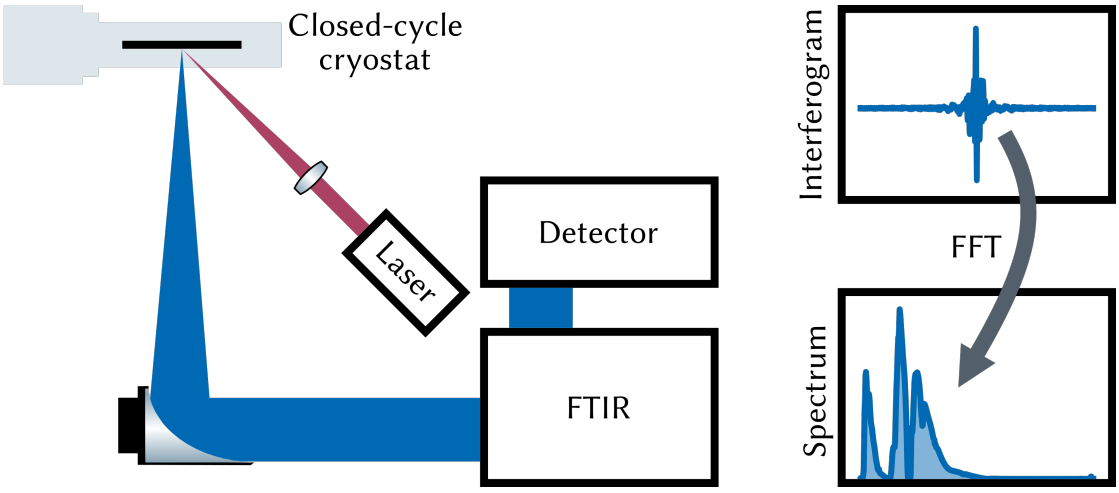

Fig. 3.2: Schematic of the FTIR PL experiment.

ogram is transformed in the respective spectrum. The spectral resolution can be set between 0.06 meV and 8 meV depending on the scanning length of the interferometer. The optical path outside the cryostat chamber can be purged with nitrogen gas. Thus, air absorption is eliminated and the optical throughput is enhanced.

3.2 Photoluminescence Excitation Spectroscopy

Photoluminescence excitation spectroscopy is a versatile method to gather absorption-like information on semiconductor heterostructures. Photoluminescence excitation is a type of PL whereby the wavelength of the excitation light is varied. The emission intensity I_{em} can be linked with the excitation intensity I_{ex} via (according to Ref. [37])

$$I_{em} = p_{abs} p_{rel} p_{em} I_{ex}. \tag{3.1}$$

Here, p_{abs}, p_{rel}, and p_{em} are the probability of a photon being absorbed by the semiconductor, the probability that the created exciton will relax to the emitting state, and the probability of radiative recombination after the relaxation process, respectively. Since in a PLE experiment, only a single emission energy is detected, p_{em} remains constant

during the measurement. p_{rel} instead is highly dependent on the excitation energy. In a non-ideal crystal, the excitons are trapped in localized states and recombine nonradiative. In nearly defect-free semiconductors, only p_{rel} gets close to unity, since the majority of charge-carriers relax to the emitting state. For these conditions, PLE can be considered as an absorptive technique.

For the PLE measurements, the *NIR* PL line-scan setup is extended. While the detection path remains the same, a spectrally filtered super continuum laser provides the tunable excitation. This is illustrated in the PLE path of Fig. 3.1. Parabolic mirrors relay the emission of the super-continuum laser onto the 1 mm entrance slit of a 0.25 m Czerny-Turner spectrometer (grating: 300 g/mm; 1000 nm blaze). The system defines a band pass of 5 nm. The spectrally filtered light is mechanically chopped and is focused on the sample. For data-correction purpose, the intensity of the chopped light is measured using an optical power meter during each measurement sequence. During the measurement, the PL is detected at a fixed energy while the excitation energy is tuned in line-scan technique. The raw data have to be corrected regarding different excitation densities due to the nonlinear emission of the super-continuum laser, the nonlinear optical response of the monochromator, and the nonlinear optical response of the detection system.

3.3 Photomodulation Spectroscopy

Instead of directly measuring an optical spectrum, the derivative of this spectrum with respect to intrinsic sample parameters can be measured by modulation spectroscopy. In this way, signatures in the linear optical response are considerably enhanced. Modulation spectroscopy utilizes the periodic perturbation of a semiconductor regarding, i.e., the sample temperature, the built-in strain, or the internal electric field.[38–41] The perturbation of the latter can be realized by illuminating the sample with a chopped laser beam.[42,43] This version of electromodulation (EM) is commonly called photomodulation. Higher photon energies than the band gap of the investigated semiconductor ($\hbar\omega > E_g$) generate electron-hole pairs, which are separated at the sample surface due to the surface electric field. This leads to a change in occupation of the surface states.[42] For samples with an internal interface the interface states are altered by the

Table 3.1: Critical points and their corresponding parameter m.

m	Critical Point
2	Excitonic
2.5	3-dimensional
3	2-dimensional

modulation. Thereby, the electric field at interfaces is modulated. Within this work photomodulated reflectance (PR) as well as photomodulated transmittance (PT) spectra are measured.

PR spectra can be categorized in three regimes, depending on the strength of the external electric field used for the modulation.[44] For this categorization, the lifetime broadening (Γ) is compared to the electro-optic energy ($\hbar\Omega$). The electro-optic energy is the characteristic energy obtained in the quantum mechanical solution of a particle of mass which is accelerated in an electric field.[45] It is given by

$$\hbar\Omega = \left(\frac{q^2\hbar^2F^2}{2\mu}\right)^{1/3}, \tag{3.2}$$

where q is the elementary charge, $\hbar$ is the Planck constant, F is the applied electric field, and μ is the interband effective mass. The low field limit is defined as $|\hbar\Omega| \leq \Gamma$ and is the relevant regime for this thesis, since the applied field strengths fulfill this criterion. In this low field regime, PR spectra can be fitted by Aspnes' empiric third derivative function:[44]

$$\frac{\Delta R}{R} = \sum_j Re\left[C_j e^{i\phi_j}\left(E - E_{g,j} + i\Gamma_j\right)^{-m}\right]. \tag{3.3}$$

The amplitude and phase factor of this Lorentzian oscillator are C and ϕ, respectively, E_g is the energy of the critical point (CP), Γ the lifetime broadening, and m defines the type of the optical transition (corresponding values of m are listed in Tab. 3.1 according to Ref. [44]). For spectrally overlapping optical transitions, one finds the modulus of a PR line shape. This modulus more clearly illustrates the contributions of particular optical transitions. It is defined by

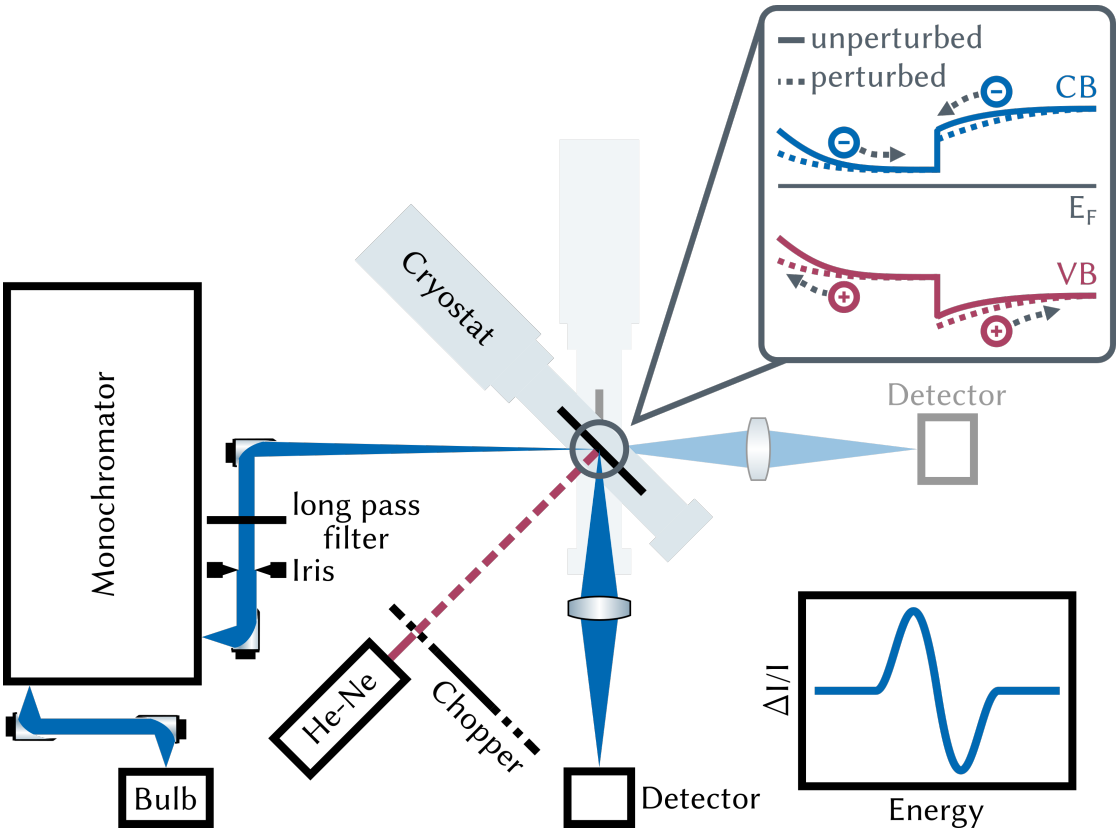

Fig. 3.3: Experimental setup of the PR and PT. The latter is grayed out.

$$\rho(E) = \sum_j \frac{|C_j|}{((E - E_{g,j})^2 + \Gamma_j^2)^{m/2}}. \tag{3.4}$$

A sketch of the line-scan PR (PT) setup is depicted in Fig. 3.3. Light of a 250 W tungsten-halogen bulb is focused onto the 1 mm entrance slit of a 1 m Czerny-Turner monochromator (grating: 600 g/mm; 1250 nm blaze). The dispersion of this configuration results in a spectral resolution of 1.5 nm and defines the band pass for the line-scan measurements. The monochromatized light is then focused onto the sample, which is mounted in the cryostat. The emission of a mechanically chopped He-Ne laser (633 nm; 2.5 mW) is spatially overlapped with the spot of the monochromatized light. This spot is then imaged on a two-stage thermoelectric cooled gallium indium arsenide (Ga(In,As)) PIN photodiode. Phase-sensitive lock-in technique is used to measures both, modulated reflectance (modulated transmittance) and reflectance (transmittance). The experimental

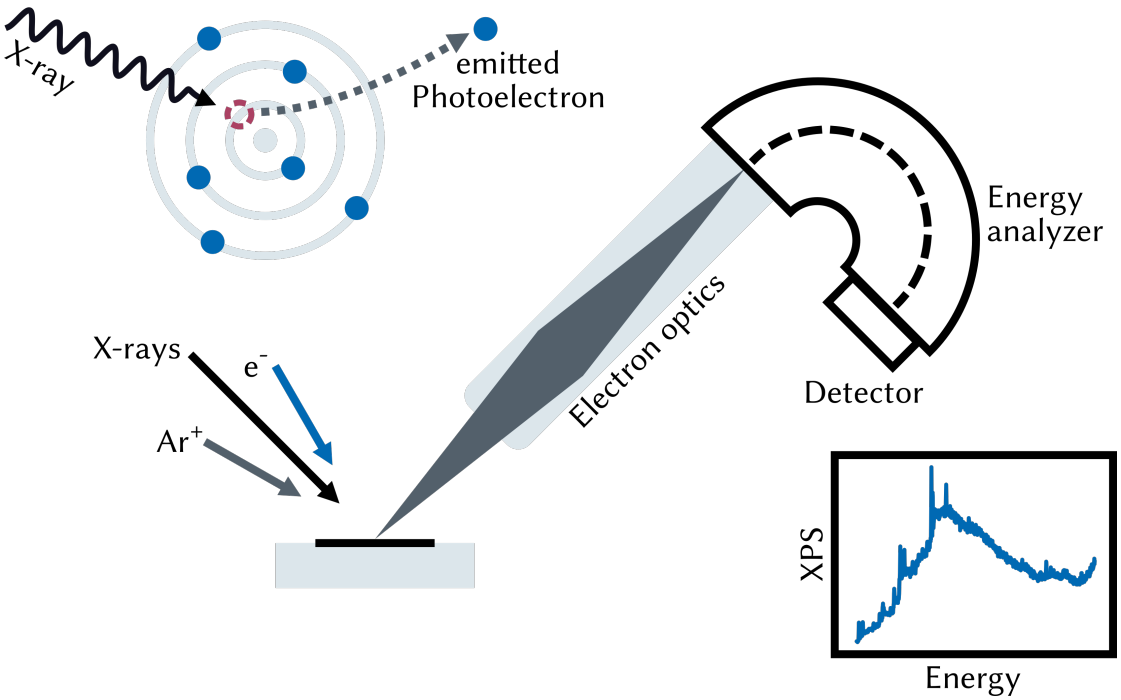

Fig. 3.4: Illustration of the XPS setup. The ionization process triggered by X-ray excitation and leading to the photoelectron emission is sketched in the upper left corner.

setup in this configuration enables measurements in a spectral range from 0.56 eV (2200 nm) up to 1.55 eV (800 nm).

3.4 X-Ray Photoelectron Spectroscopy

Electron spectroscopy is an element-sensitive tool for material analysis.[46,47] X-rays ionize the material and thus, the energy of the emitted photoelectrons is measured to determine core levels experimentally (illustrated in Fig. 3.4). Due to chemical shifts of the core levels originating, e.g., from oxidation, XPS is sensitive to oxidation states.[48] However, the peak analysis of the particular species needs to be done properly. First, the raw data has to be corrected regarding, e.g., the energy response function of the XPS setup, the electron inelastic mean free path length, or the different cross sections appropriate for the specific atomic species.[49–54] Second, to deconvolute the peaks, element specific core level energies, oxidization energies, spin-orbit splitting energies, as

Table 3.2: The spin-orbit coupling parameters define the intensity ratio of the XPS doublet peaks.

Subshell	l	s	j=l±s	Intensity ratio 2j+1
s	0	1/2	1/2	-
p	1	1/2	1/2, 3/2	1:2
d	2	1/2	3/2, 5/2	2:3
f	3	1/2	5/2, 7/2	3:4

well as intensity ratios between spin-orbit splitted subshells have to be considered.[55–58] The latter originates from spin-orbit coupling parameters and are listed in Tab. 3.2, according to Ref. [59].

XPS measurements are carried out using a PHI VersaProbe 5000 (Physical Electronics, Japan). The experimental procedure is illustrated in Fig. 3.4. The aluminum (Al) K_α-anode emitts X-rays with an energy of 1486.8 eV.[60] The X-ray emission is monochromatized by Bragg scattering on a quartz crystal in order to suppress X-ray emission from other core levels as well as Bremsstrahlung. In the analysis chamber, the monochromatized X-rays are focused onto the sample. Additionally, an electron flood gun neutralizes the surface of isolating samples. Due to the high energy of the X-rays, the penetration depth is only a few layers of atoms and, thus, XPS is a surface sensitive method. To enable depth profiles, an Ar^+ ion gun can be used for sputtering. These depth profiles are realized by a sequentially sputter process followed by the actual XPS measurements. This procedure allows to investigate deeper layers of the specimen, since the ion bombardment removes material. Here, it is inevitable to know the sputter rate of the investigated material to obtain the depth information. Electron lenses image the emitted photoelectrons onto the entrance slit of the concentric hemispherical analyzer (CHA). Here, the electrons are dispersed by an inner and outer potential forming a Wien filter. The data is digitized by a multichannel detector.

CHAPTER 4

CONCLUSION & OUTLOOK

Two concepts of novel near- and mid-IR optoelectronic materials on the basis of dilute bismuthide III-V semiconductors are investigated within the framework of this thesis. Different methods of optical and electron spectroscopy are utilized (cf. Chap. 3) for this purpose.

Ga(N,As)/ Ga(As,Bi) heterostructures on the GaAs platform yield a type-II band alignment. Asymmetric Ga(N,As)/ Ga(As,Bi) and symmetric Ga(N,As)/ Ga(As,Bi)/ Ga(N,As) heterostructures are investigated. Preliminary work deals with the improvement of the epitaxial growth of such alloys. The optimization process can be categorized in two main parts: (1) optimization of the Ga(As,Bi) layer, and (2) smoothing of the interface and symmetrization of the heterostructures. A growth interruption after the growth of the first Ga(N,As) layer allows the reactor to cool down and, thus, to ensure wafer temperatures below 450°C, since Bi incorporation requires comparably low growth temperatures. Surface wetting with the Bi precursor before deposition establishes a gradient-free growth of the Ga(As,Bi) layer and superior optical quality. However, residual Bi atoms on the growth surface hinder the N incorporation and, thus, inhibit the symmetric growth of the second Ga(N,As) layer. The wafer is heated up after the growth of the Ga(As,Bi) layer to desorb any residual Bi atoms. These steps are used to realize the heterostructures for the subsequent analysis.
The first study (publication 1) aims for a deeper understanding of the individual contributions of the two different layers by means of the type-II recombination. The analysis of the disorder signatures and the charge-carrier recombination-paths reveal, that, for

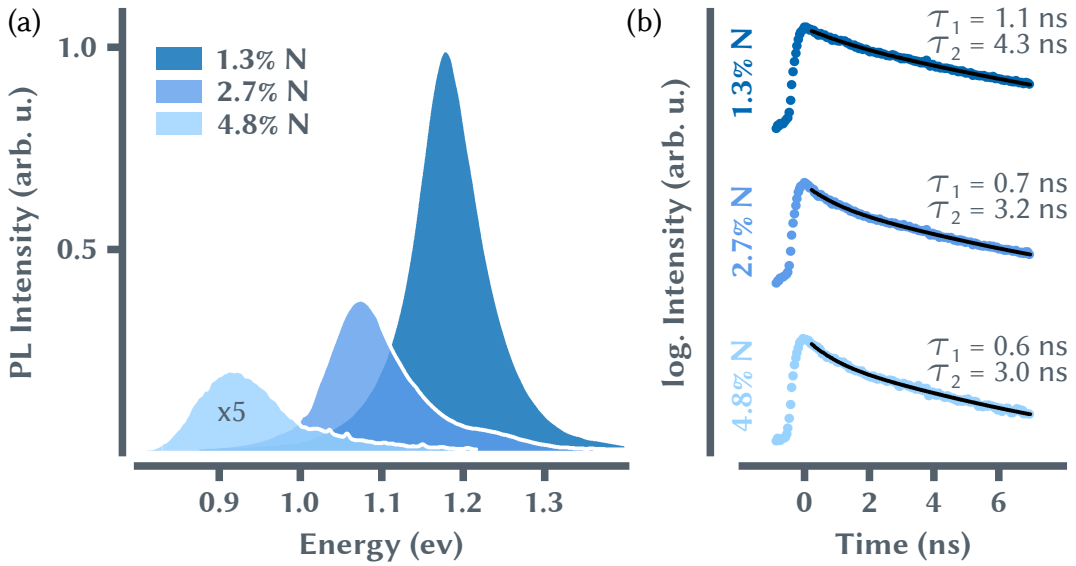

Fig. 4.1: The room-temperature PL of the W-structures (a) shows a distinct decrease of the emission energy with increasing N fraction. Time-resolved PL data are obtained at 4 K. The transients (blue circles, (b)) of the type-II transition exhibit a bi-exponential decay with faster decay times for higher N fractions. The black solid line corresponds to the fits.

both, symmetric and asymmetric type-II samples, the electron layers mainly influence the PL maxima, while the hole layer influence the linewidth. The origin of the broad linewidth was found in localized tail-states in the Ga(As,Bi) layer. The comparison between the disorder signatures of the symmetric and the asymmetric type-II structure demonstrates a larger influence of the Ga(N,As) layers on the symmetric alloy. Simultaneously, the symmetric QW structure is less influenced by disorder and, thus, exhibits a higher optical quality, i.e. the s-shape is less pronounced. PLE spectroscopy shows that electrons being absorbed in the GaAs and Ga(N,As) layers contribute more to the recombination via the type-II transition than electrons absorbed in the Ga(As,Bi) layer. This is explained by the localized states in the Ga(As,Bi) layer, since the charge carriers created directly in this layer are trapped in these states rather than relaxing towards the type-II transition.

The band-offsets forming the type-II transition are of major interest. Altering the band alignment will not only influence the emission energy but also the Auger recombination rate. Experimental observations hint the influence of the N fraction on the band alignment and, further, the capability of W-structures as emitters in data-

communication applications (Fig. 4.1 (a)). Here, the N fraction of the Ga(N,As) layers is increased from 1.3 % up to 4.8 %. This causes a distinct shift of the luminescence energy but, simultaneously, a decrease of the emission intensity. Additionally, the decay times decrease for increasing N fractions (Fig. 4.1 (b)). This results indicate higher disorder in the Ga(N,As) layers if the amount of incorporated N is increased and, thus, a higher phonon-scattering probability. Therefore, the nature of non-radiative recombination needs to be clarified and, with this in mind, whether the band alignment reduces or increases Auger recombination.

The second material system investigated is the quaternary semiconductor (Ga,In)(As,Bi) that extends the accessible spectral range further into the IR. Here, the interaction between the Bi atoms and other atomic specimen on the growth surface, their influence on the surface kinetics, and the resulting optical properties of the layers is studied. XPS measurements enable a correlation of the Ga and Bi partial pressure with the Bi surface coverage. Additionally, the surfactant effect of the Bi atoms affect the carrier temperatures. Thus, the growth parameters, in particular Ga and Bi precursor partial pressures, and disorder signatures are directly linked. In the future, the interplay between Bi and In during the sample deposition has to be investigated. The strong influence of the Bi surface coverage on the In incorporation makes the growth process even more complex. A better understanding of this specific correlation enables a higher flexibility and reliability in the heterostructure design.

PUBLICATIONS

This chapter provides the original publications which provide the highlights of the scientific work of my thesis. My own contributions to each paper are described in the paragraph of the respective publication.

Publication 1: *Comparison of Carrier-Recombination in Ga(As,Bi)/ Ga(N,As) – Type-II Quantum Wells and W-type Heterostructures*

Summary:
The realization of efficient semiconductor lasers on GaAs substrates operating at 1.55 µm and beyond remains a technological challenge. As potential solution, epitaxial heterostructures with type-II band alignment are currently discussed as active region. Each individual layer in such heterostructures features a comparably large band gap energy; therefore, spurious effects in laser operation such as reabsorption, multi-photon absorption or Auger scattering are expected to be suppressed. The actual laser operation occurs across the internal interfaces as the electron and hole wave functions have their extrema in adjacent layers. Hence, a large wave-function overlap is key for efficient recombination. A direct comparison of symmetric and asymmetric Ga(N,As)/ Ga(As,Bi) type-II quantum well heterostructures reveals that the symmetry of the layer arrangement drastically influences the charge-carrier recombination: disorder in the Ga(As,Bi) layer has more prominent effects for the asymmetric configuration compared to the symmetric one. The temperature dependence of the emission energy is mainly influenced by the Ga(N,As)-electron layers, while the temperature dependence of the full width at half maximum as well as the excitation dependence of the emission energy are dominated by the Ga(As,Bi)-hole layers. Photoluminescence excitation spec-

troscopy reveals the corresponding carrier-relaxation paths to the type-II transition.

Own contribution:
I took major parts in planning and conceptualization of this project in general with particular focus on the spectroscopy experiments. Especially the idea to use PLE spectroscopy to identify the recombination paths of the type-II structures as well as the complete planning of the PLE experiment and its components was driven by me. I planned and implemented the PLE setup. Additionally, I significantly upgraded the PL setup to perform temperature-dependent measurements as well as excitation-density dependent measurements. Data acquisition and interpretation of the temperature dependent and excitation-density dependent PL, and of the PLE was planned and performed by me. A skeleton including the results was created, which led to this publication. Here, I wrote the original manuscript and created the figures. Project administration and communication was led by me.

Applied Physics Letters ARTICLE scitation.org/journal/apl

Comparison of carrier-recombination in Ga(As,Bi)/Ga(N,As)-type-II quantum wells and W-type heterostructures

Cite as: Appl. Phys. Lett. **118**, 052103 (2021); doi: 10.1063/5.0036073
Submitted: 2 November 2020 · Accepted: 20 January 2021 ·
Published Online: 2 February 2021

Julian Veletas,[1,a)] Thilo Hepp,[2] Florian Dobener,[1] Kerstin Volz,[2] and Sangam Chatterjee[1]

AFFILIATIONS

[1]Institute of Experimental Physics I and Center for Materials Research, Justus-Liebig-University Giessen, Heinrich-Buff-Ring 16, 35392 Giessen, Germany
[2]Faculty of Physics and Materials Sciences Center, Philipps-Universität Marburg, Hans-Meerwein-Str. 6, 35035 Marburg, Germany

[a)]Author to whom correspondence should be addressed: julian.veletas@exp1.physik.uni-giessen.de

ABSTRACT

The realization of efficient semiconductor lasers on GaAs substrates operating at 1.55 μm and beyond remains a technological challenge. As a potential solution, epitaxial heterostructures with type-II band alignment are currently discussed as an active region. Each individual layer in such heterostructures features a comparably large bandgap energy; therefore, spurious effects in laser operation such as reabsorption, multi-photon absorption, or Auger scattering are expected to be suppressed. The actual laser operation occurs across the internal interfaces as the electron and hole wave functions have their extrema in adjacent layers. Hence, a large wave-function overlap is key for efficient recombination. A direct comparison of symmetric and asymmetric Ga(N,As)/Ga(As,Bi) type-II quantum well heterostructures reveals that the symmetry of the layer arrangement drastically influences the charge-carrier recombination: disorder in the Ga(As,Bi) layer has more prominent effects for the asymmetric configuration compared to the symmetric one. The temperature dependence of the emission energy is mainly influenced by the Ga(N,As)-electron layers, while the temperature dependence of the full width at half maximum and the excitation dependence of the emission energy are dominated by the Ga(As,Bi)-hole layers. Photoluminescence excitation spectroscopy reveals the corresponding carrier-relaxation paths to the type-II transition.

Conventional near- and mid-infrared lasers on the InP or the GaSb platforms suffer from intrinsic loss channels such as Auger recombination or carrier leakage.[1–3] One approach to reduce such detrimental losses significantly and, additionally, migrating these infrared light emitting devices onto GaAs substrates is using a sequence of spatially indirect (type-II) transition between adjacent layers.[4,5] Such type-II heterostructures serve as active regions in infrared laser structures. They provide vast flexibility in an emission energy design by variation of the elemental composition. For example, Ga(N,As) and Ga(As,Bi) layers may act as electron quantum wells (QWs) and hole QWs, respectively. Recently, dilute Bi-containing semiconductors are gaining increasing interest[6–10] since the incorporation of bismuth into GaAs results in a rapid decrease in the bandgap.[11–14] In a band anti-crossing picture where the isoelectronic Bi level interacts with the upper valence bands (VBs) associated with GaAs, this shift is predominantly weighted on them.[15–17] Nitrogen atoms, on the other hand, induce a large shift of the conduction band (CB) if incorporated into GaAs, again decreasing the bandgap of the GaAs host.[18–20] These specific attributes of the type-I QWs lead to a flexible design regarding the type-II emission since band-offsets can, therefore, be tuned independently. Furthermore, the pseudomorphic growth of Ga(N,As)/[Ga(As,Bi)] leads to a tensile (compressive) strained layer on GaAs. This offers the possibility for strain-balanced heterostructures on GaAs substrates.[21]

Here, we perform early stage investigations on such type-II structures that are desired for use as active medium in surface emitting lasers. Temperature-dependent photoluminescence (PL) spectroscopy provides access to the fundamental emission properties of III–V semiconductors. Additionally, the temperature dependencies reveal disorder effects and, thus, enable in-depth studies on localized states of the structures constituents. Additionally, excitation-density-dependent PL data provide information on state filling effects and tail states. Photoluminescence excitation spectroscopy (PLE) as an absorption-like technique not only provides information on oscillator strength but also traces the carrier recombination paths of the type-II transition.

The samples are mounted in a helium-flow cryostat enabling temperature-dependent measurements from 4 K up to 400 K; this includes the range of operation temperatures of many 10s °C common to diode lasers. The sample's photoluminescence (PL) is imaged onto the 500 μm entrance slit of a 1 m Czerny-Turner spectrometer and is detected by a liquid-nitrogen cooled germanium detector using the phase sensitive line-scan lock-in technique. The system yields a spectral resolution of 2 nm. For the PL experiments, a diode-pumped continuous-wave intracavity frequency-doubled Nd:YAG laser excites the sample at 2.33 eV (532 nm). The excitation light is mechanically chopped at 109 Hz; its intensity is controlled using reflective neutral-density filters. A maximum excitation density of 11.3 kW/cm^2 is estimated on the sample. For the PLE experiments, a spectrally filtered super continuum source provides the tunable excitation. A 0.25 m Czerny-Turner-type monochromator defines a bandpass of 5 nm. The raw PLE data are corrected regarding different excitation densities due to the nonlinear emission of the super-continuum laser and the nonlinear optical response of the spectrograph.

All samples are grown in an Aixtron AIX200-GFR-MOVPE reactor and the structural parameters are verified by X-ray diffraction (XRD). The used precursors are triethylgallium (TEGa), tertiarybutylarsine (TBAs), unsymmetrical dimethylhydrazine (UDMHy), and trimethylbismuth (TMBi). A GaAs buffer layer is grown on a semi-insulating GaAs substrate to achieve a flat and reproducible surface for all samples. The asymmetric type-II sample consists of 3× Ga(N,As)/Ga(As,Bi) layers, while for the symmetric type-II sample, a second Ga(N,As) layer is introduced before the Ga(As,Bi) layer. This results in a 3× Ga(N,As)/Ga(As,Bi)/Ga(N,As) heterostructure, which is also referred to as the W-type structure. The thickness of the Ga(N,As) layer in the asymmetric Ga(N,As)/Ga(As,Bi) structure is 8 nm, while all other layers' thicknesses are 4 nm. The N or Bi fractions are 1.1% and 4.0%, respectively. Each of these stacks is capped by a thin, roughly 50 nm wide GaAs layer.

Figure 1 provides an overview of the characteristic spectral emission signatures of all samples. The normalized PL spectra (the scale factors are given next to the respective curves) at 300 K show two distinct peaks: the most pronounced luminescence feature is found at energies below the GaAs-related emission at 1.42 eV. Both the emission energies and the spectral line shapes of the Ga(N,As) and Ga(As,Bi) reference samples differ significantly. The emission from the Ga(As,Bi) reference shows strong inhomogeneous broadening and an exponentially decaying low-energy tail (blue line). This is due to extended tail states due to microscopic composition fluctuations (alloy disorder) as well as Bi clusters.[22,23] The PL from the Ga(N,As) reference sample (red line) is distinctly narrower and its low energy tail is much steeper. The PL of both the type-II sample and the W-type sample has its maximum at approximately 1.1 eV. The relative intensities of the room temperature emission are in agreement with our expectations: the type-I structures show higher intensities than the type-II structures, since they have higher oscillator strengths. The Ga(As,Bi) QW sample shows more inhomogeneous broadening and, hence, slightly lower intensities in comparison to the Ga(N,As) reference structure. The lack of wave-function overlap of electrons and holes in the spatially indirect arrangements explains the lower intensities of the type-II specimens. A direct comparison of the symmetric and asymmetric type-II structures indicates a higher overlap of electron and hole wave function in the symmetric heterostructures, which leads to higher PL-intensities. The line shape of both spatially indirect transitions inherits characteristics from the Ga(N,As) and the Ga(As,Bi) photoluminescence properties, while the actual line shapes of the type-II and the W-type samples differ slightly. We perform a detailed disorder analysis and investigate state filling and potential relaxation paths to get more insight in emission and relaxation properties.

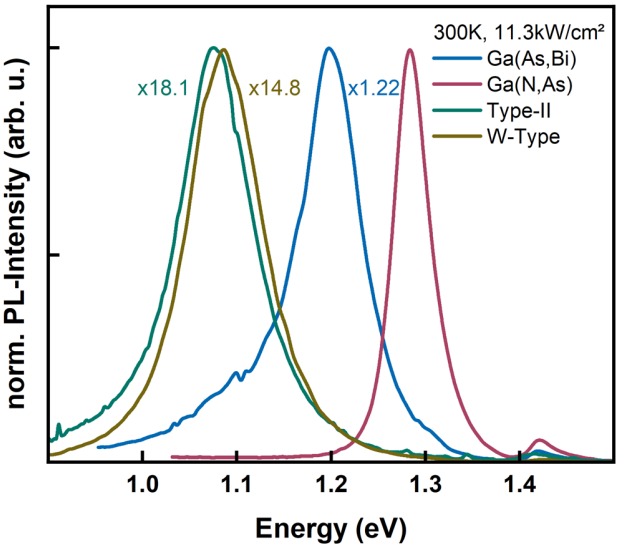

FIG. 1. PL spectra of all samples at 300 K.

Temperature-dependent PL measurements can reveal a so-called S-shape behavior in disordered type-I quantum well samples[24–26] as disorder affects their emission properties. Commonly, both the PL maximum, its full width half maximum, and its decay dynamics are affected.[27–29]

The PL-maximum energy shows a characteristic nonmonotonic behavior in energy with increasing temperature. A typical S-shape is observed, which is ascribed to thermally activated hopping processes of carriers between localized (tail-) states. This behavior is highly affected by the excitation density and is most pronounced for the lowest excitation density where least states are filled.[30] Here, excitation fluxes of 1.4 kW/cm^2 enable a full temperature-range analysis. Figure 2(a) displays the experimentally determined PL-maxima of all samples. The data are plotted as the colored squares, while the black lines act as guides to the eye. Here, the Ga(As,Bi) QW sample (blue rectangles) shows a broad disorder-related S-shape having its minimum at approximately 150 K (indicated by the blue dashed line). The local minima are reached for temperatures ranging from 50 K up to 200 K. In comparison, the Ga(N,As) QW sample's PL-maxima (red rectangles) only show a very slight S-shape with its minimum at 40 K (indicated by the red dashed line) spanning across the more narrow temperature range from 20 K to 100 K. In a straightforward approximation, the PL-maxima for the type-II and W-type samples can be assumed to be a linear superposition of the properties of the corresponding type-I reference QWs. Both the electron density-of-states (eDOS) and hole density-of-states (hDOS) should influence the spatially indirect transition between two different layers. The experimental findings support this picture for both the type-II and the W-type

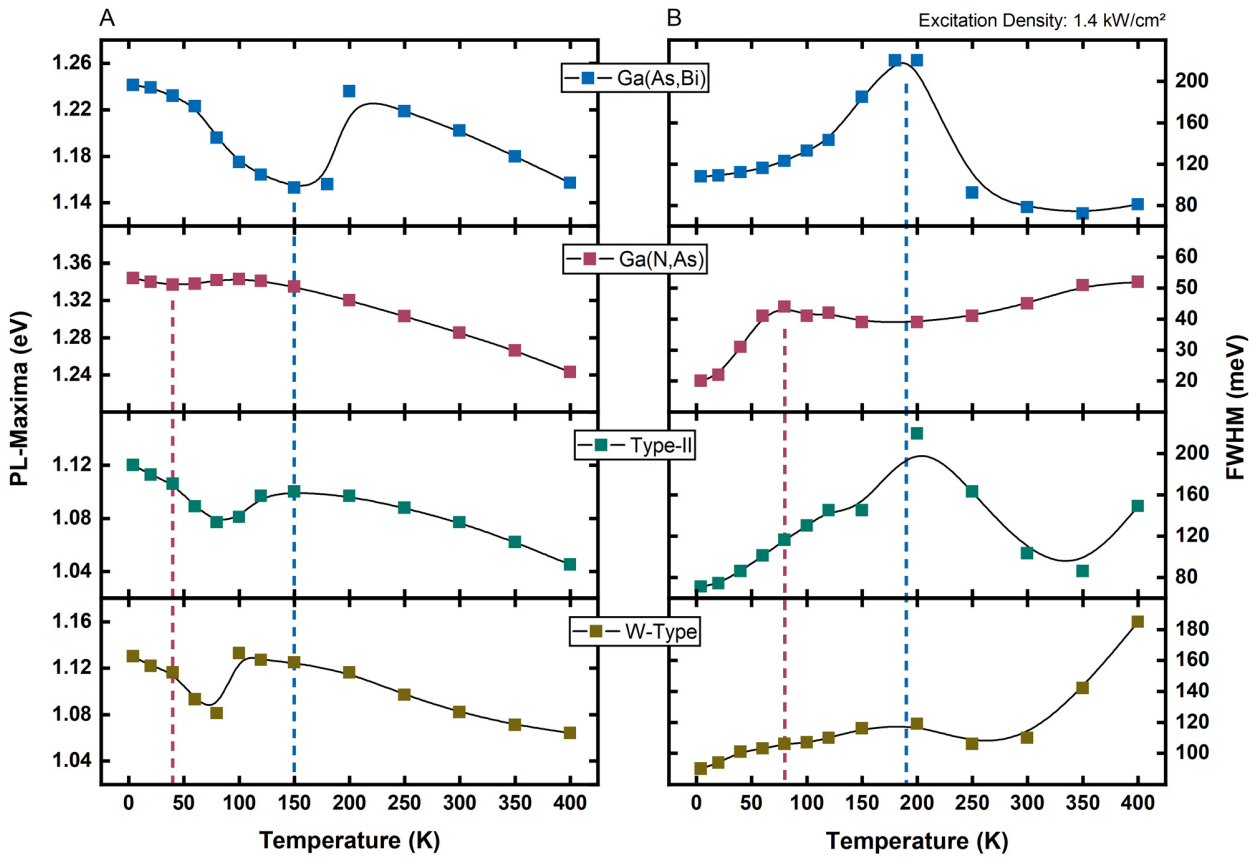

FIG. 2. Temperature dependency of the PL-maxima (a) and FWHM (b) is plotted as rectangles. The black lines are guides to the eye, while the dashed lines indicate the disorder-induced local minima (maxima) of the Ga(N,As) reference samples (red) and Ga(As,Bi) reference samples (blue) PL-maxima (FWHM).

samples. Here, the S-shape has its minimum at a temperature of 80 K and closely resembles the findings for the Ga(N,As) layer regarding the temperature shift of the PL peak position. The temperature of the local minimum of the S-shape is defined by the mobility edge of the carriers. Thus, symmetrizing the layer arrangement by introducing a second Ga(N,As) layer leads to a decrease in the mobility edge. The disorder of the Ga(As,Bi) layer influences the width of the S-shape. Nonetheless, the S-shape is more narrow for the type-II and W-type samples than for the Ga(As,Bi) QW sample. The direct comparison of the data for the type-II and the W-type sample reveals that the S-shape of the W-type sample appears to be influenced more by the Ga(N,As) layer. Two mechanisms can explain such a behavior. On the one hand, the electron wave functions are mostly located in the Ga(N,As) layers and will leak well into the Ga(As,Bi) layer by design, while the hole wave functions are well confined in the Ga(As,Bi) layer. The electron wave function in the asymmetric arrangement, however, has less overlap with the hole wave function in the Ga(As,Bi) layer than in a symmetric arrangement. On the other hand, we need to consider the joint densities-of-states for both types of heterostructures. This becomes evident when considering the combined densities-of-states for both types of heterostructures. While the asymmetric type-II structure consists of one electron-Ga(N,As) layer and one hole-Ga(As,Bi) layer, the symmetric W-type structure has two electron-Ga(N,As) layers. Both Ga(N,As) layers are not perfectly identical due to growth constraints and we have to include the possibility for nondegenerate states. Accordingly, the joint DOS for the type-II sample can be expressed approximately as $eDOS_{Ga(N,As)} \cdot hDOS_{Ga(As,Bi)}$, while the second Ga(N,As) layer has to be taken into account for the W-type structure yielding $eDOS_{Ga(N,As)modified} \cdot hDOS_{Ga(As,Bi)}$. Here, $eDOS_{Ga(N,As)modified}$ includes changes in the electron-DOS originating from the additional Ga(N,As) layer. This explains the differences observed for the samples with symmetric and the asymmetric type-II transition, respectively. PLE measurements confirm these assumptions and will be discussed below.

The analysis of the FWHM provides additional information on the electronic properties. The FWHM is shown in Fig. 2(b). Similar to the PL-maxima, the Ga(As,Bi) structure shows the strongest disorder features. The FWHM has its maximum at 190 K (indicated by the blue dashed line). The Ga(N,As) QW FWHM peaks at 80 K (red dashed line). Again for both, the type-II sample and W-type sample, the FWHM reassembles the FWHM line shape of the type-I QWs. However, the FWHM is dominated by the linewidth of the Ga(As,Bi). The electrons and holes are more separated in the asymmetric type-II

structure than in the symmetric type-II structure, as the former shows weaker confinement due to the wider Ga(N,As) layer width. The resulting difference in wavefunction overlap leads to different temperature ranges in which electrons and holes become mobile, as the corresponding wave functions have their maxima in the Ga(N,As) and Ga(As,Bi) layers, respectively. The PL spectra shown in Fig. 1 already hint different ensembles of tail states for the Ga(N,As) and the Ga(As,Bi) QW sample. The tail states of the Ga(As,Bi) layer should influence the emission of the type-II transition tremendously, due to the known disorder in the Ga(As,Bi) valence bands.[27] Temperatures above 300 K are most relevant for device operation. Here, a clear difference between the type-I and type-II samples emerges. The FWHM of the type-II and W-type samples increases rapidly in contrast to the type-I samples, which show an expected increase in the FWHM according to the carrier distribution as a function of the temperature. Most likely, the increase in the FWHM above 300 K observed for the type-II and W-type samples originates in additional transitions[31] between electron states in the Ga(N,As) layer and higher hole states in the Ga(As,Bi) layer.

The comparison of the data from the type-II sample and the W-type sample reveals a different weighting of Ga(As,Bi) and Ga(N,As) signatures in the temperature dependence of the PL. The influence of the Ga(As,Bi) disorder signatures is decreased with the introduction of a second Ga(N,As) layer. In order to further analyze the tail states of the structures, we perform excitation-density-dependent PL measurements.

The reasoning of localized states is an exponential density of states. This is illustrated in Fig. 3(a). The arrow indicates the shift of the PL maximum, while the shaded area draws the saturated states. Higher excitation-densities result in occupation of more and more of the localized states. Therefore, the PL-maximum shifts toward higher energies as a result of this state filling process.[30] The PL-maxima at 4 K as a function of excitation density are plotted in Fig. 3(b) for the type-II structures. We observe an exponential behavior of the PL-maxima for both samples. Within our experimentally accessible range, the excitation-density-dependent PL measurements expose a shift of the PL-maxima of 50 meV and 78 meV for the asymmetric and symmetric structure, respectively. This means that the slope of the DOS in the probed regime increases slower in the case of the W-type sample. We attribute this higher impact of disorder to the aforementioned differences in the two Ga(N,As) layers of the W-type structure. The PL-maxima of the reference samples are shown in Fig. 3(c) instead. The PL-maxima shift is 16 meV and 50 meV for the Ga(N,As) QW and the Ga(As,Bi) QW, respectively. Therefore, the results indicate the major role of localized states in the Ga(As,Bi) hole-layer on the disorder properties of the type-II transition. Additionally, this is in good agreement with the previous assumption that the influence on the FWHM of the Ga(As,Bi) layer originates in the tail states of the joint DOS. Within the low excitation regime, the results show that the low-energy tail states of the Ga(As,Bi) layer influence the emission of the type-II transition, since they enable transitions from excited states into localized states in the band tails.

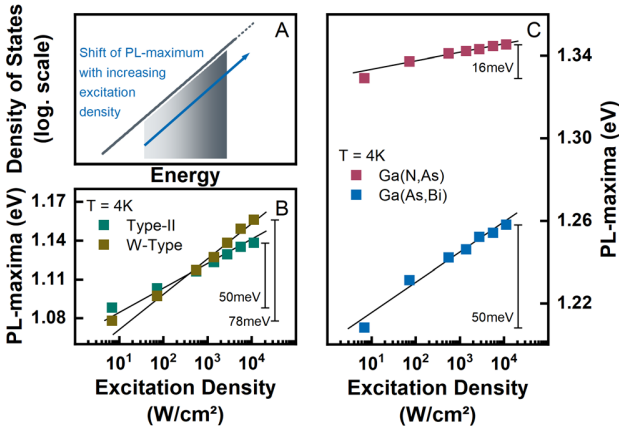

FIG. 3. The correlation between an exponential DOS and the excitation-density dependent shift of the PL-maxima is illustrated in (a). The shaded area indicates the increasing excitation density, while the blue arrow indicates the shift of the PL-maxima. The excitation-density-induced shifts of the PL-maxima at 4 K are drawn as scatter plots for the type-II structures (b) and the reference samples (c).

PLE data reveal the carrier recombination paths in type-II structures. Notably, PLE data are complex as they contain information about the absorption process, relaxation pathways, and recombination probabilities.[32] Hence, it contains information on the joint DOS and reveals which layers contribute most in feeding the spatially indirect transition in the heterostructures. Figure 4 shows PL and PLE data at a lattice temperature of 4 K as the solid line and shaded area, respectively. An additional set of PL data is taken using the super continuum laser at an emission energy of 2.33 eV (532 nm) to relate PL and PLE data. Figure 4(a) displays the spectra of the asymmetric type-II structure, and the data of the symmetric W-type structure are plotted in Fig. 4(b). Both samples have similar PL features. At 1.5 eV, the GaAs layer luminescence is detected followed by some nitrogen cluster states around 1.4 eV (Ref. 33) and the PL of the type-II transition at 1.1 eV. The dashed vertical line indicates the detection energy for the PLE measurements. While the PL line shapes are quite similar, the PLE spectra of the asymmetric and symmetric structures reveal some distinct differences. Naively, two low-energy peaks originating from the Ga(N,As) and the Ga(As,Bi) layer are expected in addition to the pronounced increase for energies above 1.5 eV associated with GaAs. Both the asymmetric and symmetric samples show a signal below energies of the GaAs regime. This signature of the Ga(N,As) layer exhibits well-known effects like Coulomb-enhancement for energies above the exciton resonances.[34] For the symmetric W-type structure, the low-energy tail of the resonance at 1.35 eV is much steeper. In addition, the resonance itself seems to be sharper than for the asymmetric structure. Again, we attribute this to the stronger carrier confinement, which results in higher absorption,[35] and to the above discussed changes in the joint DOS. The energy regime below the Ga(N,As) signature features an additional signature at approximately 1.25 eV, which is attributed to the Ga(As,Bi) layer. The PLE signal of the Ga(As,Bi) layer for the symmetric type-II arrangement below the Ga(N,As) layer energy regime is barely observable and clearly less intense than that of the asymmetric type-II arrangement. This behavior is explained by the nature of light absorption in QWs: (1) thinner QWs show stronger absorption due to the stronger carrier confinement and (2) the absorption of QWs does not depend on the amount of material but on the number of QWs.[35] Thus, for the asymmetric type-II structure, the weaker PLE signature of the Ga(As,Bi) layer can be attributed to the stronger inhomogeneous broadening, which was already observed in the temperature-dependent measurements. The

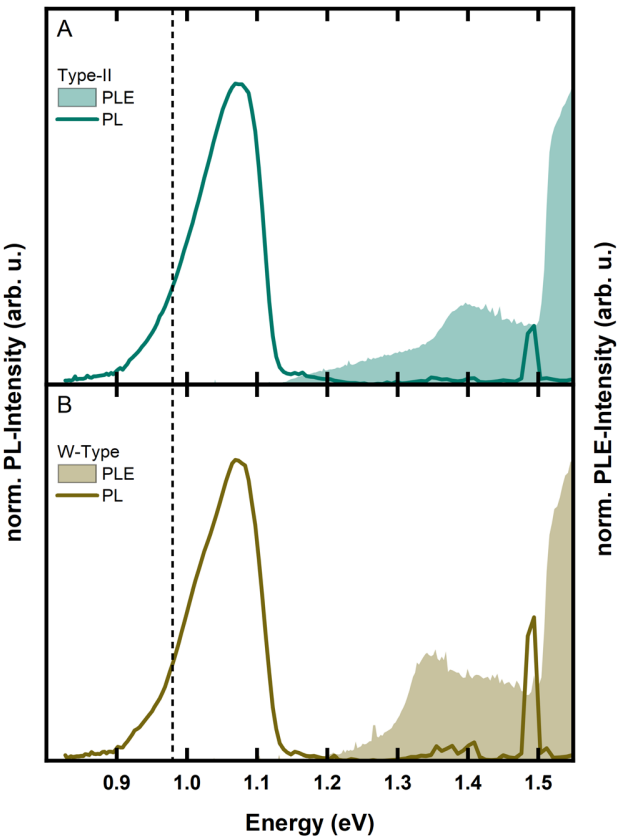

FIG. 4. Normalized PLE (shaded area) and normalized PL (solid line) data are plotted for the asymmetric (a) and symmetric (b) type-II samples. The dashed line indicates the detection energy used for the PLE measurements.

symmetric W-type structure consists of two Ga(N,As) layers, which contribute to the absorption process. Thus, the intensity of the Ga(As,Bi) layer signature compared to that of the Ga(N,As) layer signature is weaker in the W-type arrangement. The PLE data confirm the hypothesis that the changes in the combined DOS introduced by the second Ga(N,As) layer lead to these differences in PL and PLE spectra. The rather weak signature of the Ga(As,Bi) layers suggests that the electrons excited directly in the Ga(As,Bi) layer contribute insignificantly to the recombination via the type-II transition in both cases. The carriers recombining via the type-II transition are excited mostly in the GaAs barriers or in the Ga(N,As) electron-layers. We, hence, assume that the carriers excited directly in the Ga(As,Bi) layers are mostly trapped in localized states and, thus, cannot contribute to the type-II transition.

In summary, the analysis of the disorder signatures and the carrier recombination paths allows a clear distinction between the influences of the disorder properties of the emission of the two species of layers on the type-II recombination. The Ga(N,As) and Ga(As,Bi) layers feature a distinct behavior regarding their temperature-dependency of both PL maximum and FWHM. The spatially indirect transition for both the symmetric and asymmetric layer configurations inherits properties evident for the type-I reference quantum wells. This enables an assignment of the influence of the layers' materials properties on the type-II recombination. For both spatially indirect samples, the electron layers mainly influence the PL maxima dependence on temperature and excitation density, while the hole layers influence the corresponding FWHM. These results are in good agreement with straight-forward considerations taking into account that holes feature larger effective masses than electrons and are, hence, more confined in the Ga(As,Bi) layer. Thus, they have less impact on the recombination across the interface. Excitation-density-dependent PL data reveal the origin of the disorder signatures as localized tail states in the Ga(As,Bi) hole layers. The Ga(N,As) electron layer influences the symmetric W-type heterostructure more than the asymmetric one. These observations are conclusively explained when considering the respective DOS'. The carriers excited in the Ga(N,As) layer and GaAs barrier contribute more to the type-II transition than the Ga(As,Bi) layer. The valence bands of the latter are dominated by localized states. Thus, the charge carriers created directly in the Ga(As,Bi) layer are trapped in these states and, hence, contribute less to the recombination across the type-II interface.

Our results provide important implications for lasing applications utilizing such W-type arrangements. The rise of the FWHM at temperatures above 300 K is crucial for the minimum threshold current needed for lasing, since it increases the amount of states that have to be filled before reaching the inversion regime. A stronger carrier confinement in the electron and hole layers can probably shift the higher order type-II transitions out of the operation temperature regime of future devices. Nonetheless, at higher carrier densities, we expect these Ga(N,As)/Ga(As,Bi) heterostructures to perform more efficient, since disorder plays a minor role and the stronger electrostatic attraction between electrons and holes in adjacent layers improves their spatial overlap.

This work was supported by the German Research Foundation (GRK 1782: Functionalization of Semiconductors) and the Center for Materials Research (No. ZfM/LaMa). S.C. acknowledges support through the Heisenberg program (No. CH660/8).

DATA AVAILABILITY

The data that support the findings of this study are available from the corresponding author upon reasonable request.

REFERENCES

[1]G. N. Childs, S. Brand, and R. A. Abram, "Intervalence band absorption in semiconductor laser materials," Semicond. Sci. Technol. **1**, 116–120 (1986).
[2]S. J. Sweeney, A. R. Adams, M. Silver, E. P. O'Reilly, J. R. Watling, A. B. Walker, and P. J. A. Thijs, "Dependence of threshold current on QW position and on pressure in 1.5 μm InGaAs(P) lasers," Phys. Status Solidi B **211**, 525 (1999).
[3]A. D. Andreev and E. P. O'Reilly, "Theoretical study of Auger recombination in a GaInNAs 1.3 μm quantum well laser structure," Appl. Phys. Lett. **84**, 1826 (2004).
[4]G. G. Zegrya and A. D. Andreev, "Mechanism of suppression of Auger recombination processes in type-II heterostructures," Appl. Phys. Lett. **67**, 2681 (1995).
[5]G. G. Zegrya and A. F. Andreev, "Theory of the recombination of nonequilibrium carriers in type-II heterostructures," J. Exp. Theor. Phys. **82**, 2 (1996).
[6]W. Walukiewicz and J. M. O. Zide, "Highly mismatched semiconductor alloys: From atoms to devices," J. Appl. Phys. **127**, 010401 (2020).

[7]T. Hepp, O. Maßmeyer, D. A. Duffy, S. J. Sweeney, and K. Volz, "Metalorganic vapor phase epitaxy growth and characterization of quaternary (Ga,In) (As,Bi) on GaAs substrates," J. Appl. Phys. **126**, 85707 (2019).
[8]C. A. Broderick, M. Usman, E. P. O'Reilly, W. Xiong, and S. J. Sweeney, "Band engineering in dilute nitride and bismide semiconductor lasers," Semicond. Sci. Technol. **27**, 094011 (2012).
[9]J. Veletas, T. Hepp, K. Volz, and C. Chatterjee, "Bismuth surface segregation and disorder analysis of quaternary (Ga,In)(As,Bi)/InP alloys," J. Appl. Phys. **126**, 135705 (2019).
[10]P. Ludewig, N. Knaub, N. Hossain, S. Reinhard, L. Nattermann, I. P. Marko, S. R. Jin, K. Hild, S. Chatterjee, W. Stolz, S. J. Sweeney, and K. Volz, "Electrical injection Ga(AsBi)/(AlGa)As single quantum well laser," Appl. Phys. Lett. **102**, 242115 (2013).
[11]S. Francoeur, M.-J. Seong, A. Mascarenhas, S. Tixier, M. Adamcyk, and T. Tiedje, "Band gap of GaAsBi, $0 < x < 3.6\%$," Appl. Phys. Lett. **82**, 3874 (2003).
[12]S. Tixier, M. Adamcyk, T. Tiedje, S. Francoeur, A. Mascarenhas, P. Wei, and F. Schiettekatte, "Molecular beam epitaxy growth of $GaAs_{1-x}Bi_x$," Appl. Phys. Lett. **82**, 2245 (2003).
[13]N. A. Riordan, C. Gogineni, S. R. Johnson, X. Lu, T. Tiedje, D. Ding, Y. H. Zhang, R. Fritz, K. Kolata, S. Chatterjee, K. Volz, and S. W. Koch, "Temperature and pump power dependent photoluminescence characterization of MBE grown GaAsBi on GaAs," J. Mater. Sci. **23**, 1799 (2012).
[14]J. Hader, S. C. Badescu, L. C. Bannow, J. V. Moloney, S. R. Johnson, and S. W. Koch, "Extended band anti-crossing model for dilute bismides," Appl. Phys. Lett. **112**, 062103 (2018).
[15]K. Alberi, O. D. Dubon, W. Walukiewicz, K. M. Yu, K. Bertulis, and A. Krotkus, "Valence band anticrossing in $GaBi_xAs_{1-x}$," Appl. Phys. Lett. **91**, 051909 (2007).
[16]S. Imhof, C. Bückers, A. Thränhardt, J. Hader, J. V. Moloney, and S. W. Koch, "Microscopic theory of the optical properties of Ga(AsBi)/GaAs quantum wells," Semicond. Sci. Technol. **23**, 125009 (2008).
[17]K. Alberi, J. Wu, W. Walukiewicz, K. M. Yu, O. D. Dubon, S. P. Watkins, C. X. Wang, X. Liu, Y.-J. Cho, and J. Furdyna, "Valence-band anticrossing in mismatched III-V semiconductor alloys," Phys. Rev. B **75**, 045203 (2007).
[18]P. J. Klar, H. Grüning, W. Heimbrodt, J. Koch, F. Höhnsdorf, W. Stolz, P. M. A. Vicente, and J. Camassel, "From N isoelectronic impurities to N-induced bands in the GaN_xAs_{1-x} alloy," Appl. Phys. Lett. **76**, 3439 (2000).
[19]W. Shan, W. Walukiewicz, K. M. Yu, J. W. Ager, E. E. Haller, J. F. Geisz, D. J. Friedman, J. M. Olson, S. R. Kurtz, H. P. Xin, and C. W. Tu, "Band anticrossing in III-N-V alloys," Phys. Status Solidi B **223**, 75 (2001).
[20]T. Taliercio, R. Intartaglia, B. Gil, P. Lefebvre, T. Bretagnon, U. Tisch, E. Finkman, J. Salzman, M.-A. Pinault, M. L. Gt, and E. Tournié, "From GaAs:N to oversaturated GaAsN: Analysis of the band-gap reduction," Phys. Rev. B **69**, 73303 (2004).
[21]C. A. Broderick, S. Jin, I. P. Marko, K. Hild, P. Ludewig, Z. L. Bushell, W. Stolz, J. M. Rorison, E. P. O'reilly, K. Volz, and S. J. Sweeney, "$GaAs_{1-x}Bix/GaNyAs_{1-y}$ type-II quantum wells: Novel strain-balanced heterostructures for GaAs-based near- and mid-infrared photonics," Sci. Rep. **7**, 1–9 (2017).
[22]S. Francoeur, S. Tixier, E. Young, T. Tiedje, and A. Mascarenhas, "Bi isoelectronic impurities in GaAs," Phys. Rev. B **77**, 085209 (2008).
[23]C. Gogineni, N. A. Riordan, S. R. Johnson, X. Lu, and T. Tiedje, "Disorder and the Urbach edge in dilute bismide GaAsBi," Appl. Phys. Lett. **103**, 041110 (2013).
[24]S. D. Baranovskii, R. Eichmann, and P. Thomas, "Temperature-dependent exciton luminescence in quantum wells by computer simulation," Phys. Rev. B **58**, 13081 (1998).
[25]C. Karcher, K. Jandieri, B. Kunert, R. Fritz, M. Zimprich, K. Volz, W. Stolz, F. Gebhard, S. D. Baranovskii, and W. Heimbrodt, "Peculiarities of the photoluminescence of metastable Ga(N,As,P)/GaP quantum well structures," Phys. Rev. B **82**, 245309 (2010).
[26]V. Valkovskii, K. Jandieri, F. Gebhard, and S. D. Baranovskii, "Rethinking the theoretical description of photoluminescence in compound semiconductors," J. Appl. Phys. **123**, 055703 (2018).
[27]S. Imhof, A. Thränhardt, A. Chernikov, M. Koch, N. S. Köster, K. Kolata, S. Chatterjee, S. W. Koch, X. Lu, S. R. Johnson, D. A. Beaton, T. Tiedje, and O. Rubel, "Clustering effects in Ga(AsBi)," Appl. Phys. Lett. **96**, 131115 (2010).
[28]S. Imhof, C. Wagner, A. Thränhardt, A. Chernikov, M. Koch, N. S. Köster, S. Chatterjee, S. W. Koch, O. Rubel, X. Lu, S. R. Johnson, D. A. Beaton, and T. Tiedje, "Luminescence dynamics in Ga(AsBi)," Appl. Phys. Lett. **98**, 161104 (2011).
[29]M. K. Shakfa, D. Kalincev, X. Lu, S. R. Johnson, D. A. Beaton, T. Tiedje, A. Chernikov, S. Chatterjee, and M. Koch, "Quantitative study of localization effects and recombination dynamics in GaAsBi/GaAs single quantum wells," J. Appl. Phys. **114**, 164306 (2013).
[30]V. Valkovskii, M. K. Shakfa, K. Jandieri, P. Ludewig, K. Volz, W. Stolz, M. Koch, and S. D. Baranovskii, "Excitation dependence of the photoluminescence lineshape in Ga(NAsP)/GaP multiple quantum well: Experiment and Monte-Carlo simulation," J. Phys. D **50**, 025105 (2017).
[31]S. Gies, C. Kruska, C. Berger, P. Hens, C. Fuchs, A. Ruiz Perez, N. W. Rosemann, J. Veletas, S. Chatterjee, W. Stolz, S. W. Koch, J. Hader, J. V. Moloney, and W. Heimbrodt, "Excitonic transitions in highly efficient (GaIn)As/Ga(AsSb) type-II quantum-well structures," Appl. Phys. Lett. **107**, 182104 (2015).
[32]M. Cardona and P. Y. Yu, *Fundamentals of Semiconductors*, 4th ed. (Springer, 1995).
[33]A. Lindsay and E. P. O'reilly, "Unification of the band anticrossing and cluster-state models of dilute nitride semiconductor alloys," Phys. Rev. Lett. **93**, 196402 (2004).
[34]H. Haug and S. W. Koch, *Quantum Theory of the Optical and Electronic Properties of Semiconductors* (World Scientific Publishing, 2003).
[35]P. Blood, "On the dimensionality of optical absorption, gain, and recombination in quantum-confined structures," J. Quantum Electron. **36**, 354 (2000).

Publication 2: *Bismuth surface segregation and disorder analysis of quaternary (Ga,In)(As,Bi)/ InP alloys*

Summary:
The incorporation of small fractions of bismuth atoms in III-V semiconductors such as (Ga,In)As leads to a vast decrease of the band-gap energies accompanied by an increase of the spin-orbit splitting energies of the alloy compared to the host material. This effect is commonly described by an anti-crossing of the bismuth-level with the valence bands of the matrix. Growth and characterization of quaternary alloys like (Ga,In)(As,Bi) remains challenging due to the required low growth temperatures, since Bi generally tends to have pronounced surfactant properties on the one hand and the similar influence in Bi and In on most structural, electronic and optical properties such as the lattice constant or the band gap energy.

In this study, we uniquely identify surface diffusion of the bismuth atoms with X-ray photoelectron spectroscopy and relate the finding to growth parameters and photoluminescence properties and X-ray diffraction patterns of the material. We show the influence of different partial pressures of the MOVPE growth on the bismuth segregation process as well as a consequence thereof the disorder properties of those samples compared to (Ga,In)As/ InP reference alloys.

Own contribution:
I transferred the PL setup from Marburg to Giessen, designed extensions for this setup, and implemented the new parts in the measurement software. Both, PL and XPS measurements have been carried out by me. For PL-data analysis, I used self-developed software on the basis of well established models to analyze III-V semiconductors. I evaluated the XPS data using CasaXPS. Furthermore, I took main part in the conceptualization process of the publication. I wrote the original draft of the paper and created all of the figures. Project administration and communication was led by me.

Journal of Applied Physics ARTICLE scitation.org/journal/jap

Bismuth surface segregation and disorder analysis of quaternary (Ga,In)(As,Bi)/InP alloys

Cite as: J. Appl. Phys. **126**, 135705 (2019); doi: 10.1063/1.5111913
Submitted: 31 May 2019 · Accepted: 15 September 2019 ·
Published Online: 2 October 2019

Julian Veletas,[1,a)] Thilo Hepp,[2] Kerstin Volz,[2] and Sangam Chatterjee[1]

AFFILIATIONS

[1]Institute of Experimental Physics I and Center for Materials Research, Justus-Liebig-University Giessen, Giessen DE-35392, Germany
[2]Faculty of Physics and Materials Sciences Center, Philipps-Universität Marburg, Marburg DE-35032, Germany

Note: This paper is part of the Special Topic on Highly Mismatched Semiconductors Alloys: from Atoms to Devices.
[a)]**Electronic mail:** julian.veletas@exp1.physik.uni-giessen.de

ABSTRACT

The incorporation of small fractions of bismuth atoms in III–V semiconductors such as (Ga,In)As leads to a vast decrease of the bandgap energies accompanied by an increase of the spin-orbit splitting energies of the alloy compared to the host material. This effect is commonly described by an anticrossing of the bismuth-level with the valence bands of the matrix. Growth and characterization of quaternary alloys like (Ga,In)(As,Bi) remains challenging due to the required low growth temperatures, since Bi generally tends to have pronounced surfactant properties on the one hand and the similar influence in Bi and In on most structural, electronic, and optical properties such as the lattice constant or the bandgap energy. In this study, we uniquely identify surface diffusion of the bismuth atoms with X-ray photoelectron spectroscopy and relate the finding to growth parameters and photoluminescence properties and X-ray diffraction patterns of the material. We show the influence of different partial pressures of the MOVPE growth on the bismuth segregation process as well as a consequence thereof the disorder properties of those samples compared to (Ga,In)As/InP reference alloys.

I. INTRODUCTION

Bismuth-containing semiconductors such as (Ga,In)(As,Bi) are promising material systems for infrared light emitting devices. The incorporation of small fractions of isovalent bismuth introduces a virtually dispersionless defect level within the uppermost valence bands; a process commonly described by a band anticrossing model.[1,2] This effectively leads to a decrease of the host semiconductors bandgap, e.g., by 86 meV per percent Bi incorporation into GaAs.[3] Simultaneously, the comparatively heavy Bi-atoms increase the effective atomic number which then increases the spin-orbit splitting energy.[4] Eventually, the incorporation of large enough Bi fractions are expected to decrease the bandgap energy below the spin-orbit splitting energy. Roughly, 4% are expected for the quaternary alloy (Ga,In)(As,Bi).[5] This, in turn, may lead to a suppression of the conduction band–heavy-hole band–split-off band–heavy-hole band (CHSH) Auger-recombination.[6] Those properties and the wide scope for bandgap engineering make this material system attractive for highly efficient near to midinfrared lasers based on industrial InP technology. While the ternary alloy Ga(As,Bi) is comparatively well characterized and understood, growth and characterization of quaternaries remains challenging.[7–10] For instance, the incorporation of indium and bismuth atoms both lead to similar changes in the lattice parameter and the electronic bandgap, rendering the unique identification by macroscopic, nonchemically sensitive, i.e., element specific approaches such as optical spectroscopy or x-ray diffraction virtually impossible.[11]

Here, we report on a structural and disorder analysis utilizing X-ray photoelectron spectroscopy (XPS) and temperature-dependent photoluminescence (PL) spectroscopy. We qualitatively investigate the bismuth surface diffusion as XPS resolves chemical species in different oxidization states. Additionally, combining the XPS routine with an argon ion beam bombardment probes deeper layers within the sample. We unambiguously confirm that bismuth segregation reduces disorder effects as is proposed in the literature[12,13] by analyzing the corresponding luminescence of the samples and comparing them to ternary (Ga,In)As/InP alloys. Bismuth atoms change the surface kinematics of the growing surface by suppressing island formation and, thus, the surface or interface is smoothened.

Additionally, in MOVPE, the surplus bismuth reduces unintentional C doping. The Bi-atoms block the group-V lattice sites at the surface.

II. EXPERIMENTAL DETAILS

The XPS data have been acquired using a VersaProbe 5000 (PHI, Japan) spectrometer operating with an aluminum K_α-anode (1486.8 eV). A standard angle of 45° is set between the sample surface and the detector. All spectra are acquired using beam powers of 50 W with a beam diameter of 200 μm and a pass energy of 23.50 eV. Sample neutralization is realized using a low current argon flood gun and a higher current electron flood gun in order to compensate surface charging effects. Depth profiles are generated by locally sputtering the samples between the data acquisition times using an argon ion gun set to 2 kV, 1.9 μA with a 2 mm spot size. The ion bombardment lasts 28 s for each interval. In the bulk sample, this leads to 7 nm steps for the depth profile, according to a sputter rate of 0.283 nm s^{-1} determined in previous experiments.

The PL setup features a closed-cycle helium cryostat as well as a Fourier-transform infrared spectrometer (FTIR) combined with a liquid-nitrogen-cooled InSb detector. A 650 nm laser diode excites the sample with an excitation density of 20 W cm^{-2}. All spectra are obtained under the same excitation conditions while the temperature was varied between 15 K up to 100 K except those of the (Ga,In)As sample grown at 450 °C. The latter, low temperature grown (Ga,In)As sample is excited using a 808 nm laser diode with an excitation density of 356 W cm^{-2} due to its low photoluminescence yield.

All samples have been grown in an Aixtron AIX200-GFR-MOVPE reactor. A 300 nm InP buffer layer is deposited on n-doped InP substrate at 590 °C growth temperature followed by a growth interruption allowing the deposited material to cool down. Next, the approximately 50 nm (Ga,In)(As,Bi) layer is grown at 450 °C to minimize bismuth segregation.[14] Several samples are grown using different precursors, namely, triethylgallium (TEGa), teimethylindium (TMIn), tertiarybutylarsine (TBAs), and trimethylbismuth (TMBi). In particular, TEGa/III and TMBi/V precursor flux ratios are varied, while the overall V/III ratio is kept constant at 2.7. Table I summarizes the different growth conditions of the bismuth-containing samples. For analysis of the influence of the surfactant effect on the disorder properties, we additionally investigate two (Ga,In)As/InP samples grown at similar growth conditions as the (Ga,In)(As,Bi)/InP samples. One of these samples has been grown at conventional $T_{\mathrm{growth,standard}} = 590$ °C and the other at a low temperature $T_{\mathrm{growth,low}} = 450$ °C for direct comparison to the (Ga,In)(As,Bi) alloys.

TABLE I. Varied partial pressures (pp) of the samples.

Sample	pp(TEGa)/III	pp(TMBi)/V
Ga755	0.755	0.005
Ga733	0.733	0.005
Ga706	0.706	0.005
Bi03	0.755	0.003

III. BISMUTH SEGREGATION

The inherent chemical sensitivity of XPS to the oxidation state reveals the role of surface migration, which is commonly observed for bismuth atoms due to their low solubility in GaAs-like hosts and they, hence require low growth temperatures.[15] Any Bi reaching the sample surface oxidizes when in contact with air while metallic species only persist inside the material.

Therefore, the Bi 4*f* orbitals of the samples are analyzed which show a distinct set of peaks which allow to distinguish between metallic and oxide bismuth species. The Bi 4*f* region has well separated spin-orbit components with a splitting energy of $\Delta = 5.3$ eV. The binding energies are 157 eV and 159 eV for Bi $4f_{7/2}$ and Bi_2O_3, respectively.[16] The peaks for bismuth metal have an asymmetric line shape while bismuth compounds like the oxide have symmetric peaks. Figure 1(a) shows XPS spectra of the Bi 4*f* region for the sample with the lowest pp(TEGa)/III ratio. The above-mentioned peaks are all well distinguishable. The vertical blue lines indicate the Bi 4*f* binding energies, the gray-shaded areas the Bi_2O_3 peak, and the blue-shaded areas represent the metallic bismuth species. The green-shaded area indicates the Ga 3*s* peak, laying in the same energy region than the Bi 4*f* orbital. The spectra are energy calibrated using the common C 1*s* line where the most intense line is due to the C–C bonds of carbon at 284.8 eV. A correction for the transmission function of the electron lens, inelastic mean free path length, and different cross sections appropriate for the specific atomic species is applied.[17–20] Fitting the spectra using a symmetric Voigt profile and an asymmetric Voigt profile and considering the area of the fits provides quantitative information about the ratio between the two bismuth species.[21] Reducing the Bi-flux, however, virtually eliminated the bismuth oxide peak and only metallic bismuth is found in the XPS spectra as shown in Fig. 1(c). While Figs. 1(a) and 1(c) depict spectra obtained at the samples surface, Figs. 1(b) and 1(d) show the respective signals taken after an argon ion bombardment, corresponding to a depth of 8 nm. The spectra are scaled by a factor of four. Bi_2O_3 vanishes completely in deeper sample layers. Simultaneously, the Ga 3*s* peak mostly remains its area, which is directly related to the elemental fraction. It occurs that the amount of metallic bismuth inside the samples is less than at the samples surfaces. This confirms the low solubility of bismuth atoms, concomitant with a diffusion toward the samples surface. The less intense signal is an additional indicator for only low amounts of bismuth incorporated into the crystal lattice, as it was proposed in the disorder discussion. Comparing the influence of gallium precursor partial pressures on the bismuth oxide fraction [Fig. 1(e)] reveals a clear trend. Increased Ga-fluxes decrease the rates of bismuth oxide, which may lead to an increase of incorporated bismuth. This is supported by the disorder data, since higher amounts of bismuth increase disorder signatures.

Second, XPS provides structural information on the investigated samples. In particular, depth scans of the structures qualitatively analyze the growth homogeneity and the elemental composition. Details of the applied argon ion bombardment routine is described in Sec. II. Figure 2 depicts an exemplary depth scan. The different scatter plot symbols mark the normalized compositional fraction of the group III and V elements. The InP substrate is illustrated as shaded background in the graph. The XPS spectra show very plainly

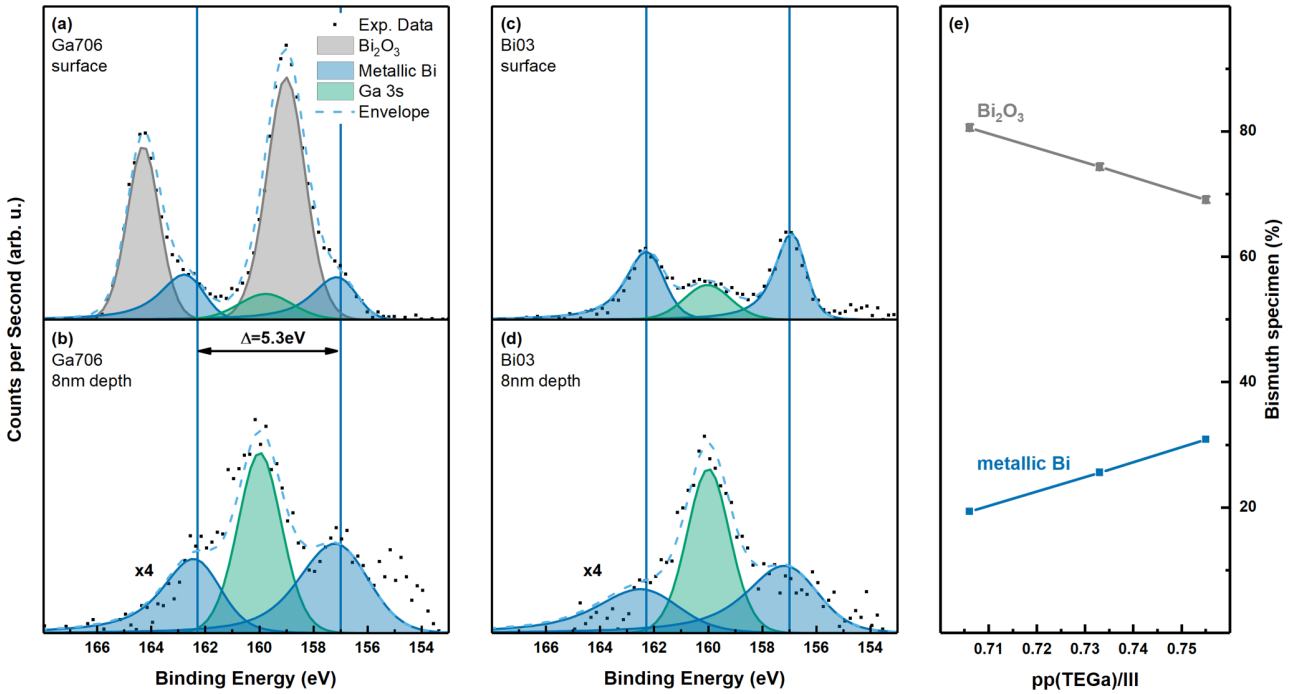

FIG. 1. XPS spectra (scatter plot) of the Bi 4*f* orbital. The gray-shaded areas shows the oxide parts of the signal, while the blue-shaded regions indicate the metallic and, thus, the incorporated part of the bismuth atoms; the green-shaded regions represent the Ga 3*s* orbitals. The vertical lines indicate binding energies of the metallic Bi 4*f* orbitals. (a) and (b) show the signature for the sample with the lowest Ga-flux on the samples surface and within 8 nm depth, respectively; (c) and (d) the spectra for the sample with reduced Bi-flux. The data in (e) show the percentage of Bi_2O_3 at the samples surface as a function of the TEGa partial pressure.

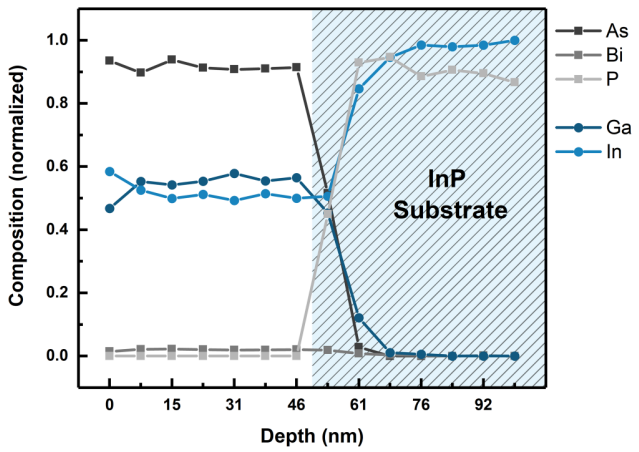

FIG. 2. Qualitative XPS depth scan, the composition of the group-V elements are shown in gray, and group III elements in blue. The shaded area indicates the InP substrate.

the interface between the (Ga,In)(As,Bi) layer and the InP substrate. The fractions of In and P converge toward the same ratio while the As, Ga, and Bi signals decay rapidly in the substrate. The nonabrupt decay of the elemental fraction originates from preferential sputtering effects for the different atom species as well as residual atoms in the sputter crater.[22] Different alloy components sputter at different rates if the energy transfer between the argon ions and the respective alloy components is not equally efficient or if their bond strength vary.[23] Unfortunately, the preferential sputtering effects distort the data most pronounced between the first two data points in each set of elements. Beside those, a nearly constant line accommodates for every single atomic species through the whole sample thickness. This shows a smooth sample layer with no interlayers nor huge composition fluctuations.

IV. QUANTIFICATION OF DISORDER EFFECTS

Temperature-dependent PL measurements provide significant insights into the optical properties of the investigated samples. The data reveal a high thermal quenching, which is attributed to surface band-bending effects as all structures are intentionally

grown without a capping layer to facilitate the XPS measurements. Analyzing the emission characteristics in more detail clarifies the potential role of disorder in these samples, in particular, for the observed thermal PL quenching. Figure 3 opposes the PL spectra of one exemplary (Ga,In)(As,Bi)/InP sample with the (Ga,In)As/InP reference. The full width at half maxima (FWHM) are easily compared on the linear scales [Figs. 3(a) and 3(b)]; it provides a measure of broadening effects due to carrier scattering.[24] Since the investigated (Ga,In)(As,Bi)/InP samples show very similar PL, we compare the Ga755 sample with the (Ga,In)As/InP sample which is grown at $T_{\mathrm{Growth}} = 590\,^{\circ}\mathrm{C}$. Here, we observe a FHWM of 7.5 meV at 15 K lattice temperature and almost double that value, i.e., 15.6 meV for the (Ga,In)As/InP and the (Ga,In)(As,Bi)/InP samples, respectively. The PL FWHM of the (Ga,In)As/InP sample grown at the same growth conditions as the quaternary alloys ($T_{\mathrm{Growth}} = 450\,^{\circ}\mathrm{C}$) is 17.7 meV at 15 K. This confirms the influence of bismuth as a surfactant during growth, since the explained surfactant effect increases the photoluminescence efficiency and reduces the amount of defects and, thus, the linewidth of the PL narrows. However, the slightly higher excitation density for the LT (Ga,In)As/InP sample due to the extremely low radiative efficiency also has to be taken into account. The higher excitation densities broaden the PL linewidth.

To get an in-depth coverage of the influence of the different partial pressures on the disorder properties, we now focus on the Planck tails of the PL. The Planck tails are the high-energy tails of the PL and provide direct information about carrier thermalization. Ideal crystals show a pure Boltzmann distribution for the carrier temperatures.[25] Defect states and disorder signatures lead to deviations from this behavior effectively leading to higher carrier temperatures.[26] In this nonideal crystals transitions to impurity related bands alter the thermalization process. Therefore, the width of the Planck tail provides a reliable measure for defect-related recombination processes. Nonetheless, this model requires a nearly constant density-of-states in the investigated spectral region. In quantum wells, the density-of-states is naturally flat due to confinement effects. Taking excitonic effects in bulk semiconductors into account, the Sommerfeld factor flattens the density-of-states in the free electron plasma regime, thus, justifying the use of this model for our analysis.[27] Figure 4(a) shows how the Planck tails are obtained out of the spectra. A linear regression is fitted at the logarithmized high-energy tail of the PL, since the carrier distribution follows $\sim\exp(-h\nu/E_p)$, where E_p is proportional to $k_{\mathrm{B}}T$ in equilibrium. The analysis of the Planck-tail widths reveals two major findings. First, we show that a reduction of the Ga-flux leads to a decrease in carrier temperatures and a better convergence toward the Boltzmann distribution as well [gray colored data in Fig. 4(b)]. Reducing the Bi-flux increases disorder signatures. This is most obviously visible in the 50 K to 100 K temperature regime. Second, we can compare the quaternary alloys with the ternary (Ga,In)As/InP samples. The high temperature grown (Ga,In)As sample shows smaller Planck-tail widths and therefore, lower carrier temperatures. This is explained by the overall more complex growth process, if bismuth is introduced into the crystal lattice. Additionally, the required low growth temperatures reinforce the formation of defects in the host crystal matrix. Interestingly, the low temperature grown (Ga,In)As sample exhibits the highest Planck-tail widths. It becomes apparent that the bismuth-induced surfactant effect enhances the crystal quality by reducing defects in the lattice. We unambiguously show that the surfactant effect of the bismuth atoms enhances the crystal quality by taking both, the FWHM and the Planck-tail widths into account and comparing them with the ternary alloys.

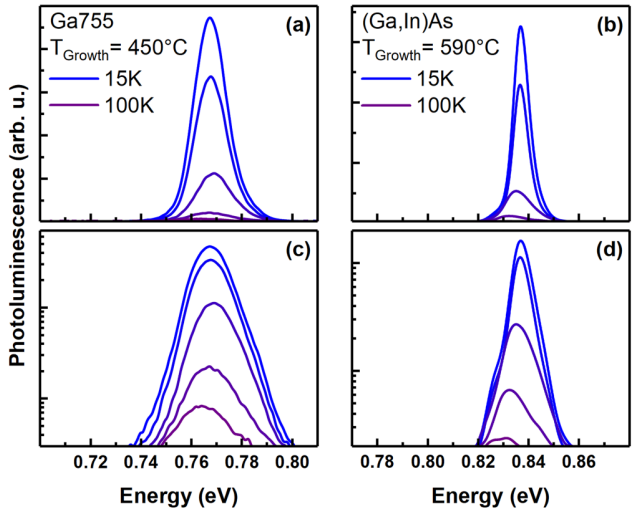

FIG. 3. Temperature-dependent photoluminescence spectra of (a) an exemplary (Ga,In)(As,Bi) sample and (b) the high temperature grown (Ga,In)As reference sample.

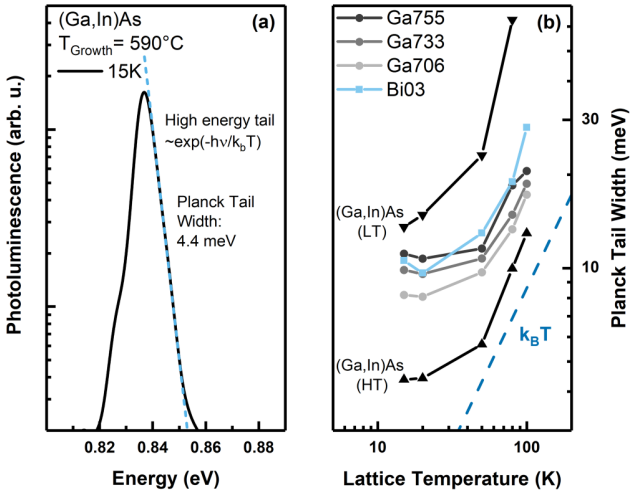

FIG. 4. (a) Illustration of PL data and exponential fit for the extraction of the Planck-tail width. (b) Width of the Planck tails derived from temperature-dependent PL measurements.

V. CONCLUSIONS

In summary, XPS is a powerful tool to investigate dilute bismuthide semiconductors. This element-sensitive method enables insight into material-specific challenges such as the segregation of bismuth atoms to the samples surface. Furthermore, it accesses intermediary layers and depth profiles in combination with an argon ion sputtering process.

Quantitative analysis of the XPS measurements shows a clear dependence of the Bi_2O_3 ratio linked to the partial pressure of both, the TEGa and the TMBi precursor, as well. This allows enhanced control of the growth of bismuthide semiconductors. Depth profiles expose homogeneous compositions without interlayers for all samples.

Optical spectroscopy reveals comparably low disorder effects and slight bismuth-induced shifts in the bandgap energy interfering that presumably only very small amounts of bismuth are incorporated which is in excellent agreement with the XPS data. The comparison with high quality (Ga,In)As/InP sample and a (Ga,In)As/InP sample grown at similar growth temperature as the (Ga,In)(As,Bi)/InP samples reveals that the surfactant effect of the bismuth atoms reduces carrier temperatures and, thus, reduces disorder signatures in the III–V alloy.

ACKNOWLEDGMENTS

This work has been supported by the German Research Foundation (No. GRK 1782: Functionalization of Semiconductors) and the Center for Materials Research (ZfM/LaMa). S.C. acknowledges support through the Heisenberg Program (No. CH660/2).

REFERENCES

[1]K. Alberi, O. D. Dubon, W. Walukiewicz, K. M. Yu, K. Bertulis, and A. Krotkus, Appl. Phys. Lett. **91**, 051909 (2007).
[2]K. Alberi, J. Wu, W. Walukiewicz, K. M. Yu, O. D. Dubon, S. P. Watkins, C. X. Wang, X. Liu, Y.-J. Cho, and J. Furdyna, Phys. Rev. B **75**, 045203 (2007).
[3]S. Francoeur, M.-J. Seong, A. Mascarenhas, S. Tixier, M. Adamcyk, and T. Tiedje, Appl. Phys. Lett. **82**, 3874 (2003).
[4]P. Carrier and S.-H. Wei, Phys. Rev. B **70**, 035212 (2004).
[5]I. P. Marko and S. J. Sweeney, Appl. Phys. Lett. **101**, 221108 (2012).
[6]C. A. Broderick, M. Usman, E. P. O'Reilly, W. Xiong, and S. J. Sweeney, Semicond. Sci. Technol. **27**, 094011 (2012).
[7]P. Ludewig, N. Knaub, N. Hossain, S. Reinhard, L. Nattermann, I. P. Marko, S. R. Jin, K. Hild, S. Chatterjee, W. Stolz *et al.*, Appl. Phys. Lett. **102**, 242115 (2013).
[8]N. A. Riordan, C. Gogineni, S. R. Johnson, X. Lu, T. Tiedje, D. Ding, Y. H. Zhang, R. Fritz, K. Kolata, S. Chatterjee *et al.*, J. Mater. Sci. Mater. Electron. **23**, 1799 (2012).
[9]M. K. Shakfa, D. Kalincev, X. Lu, S. R. Johnson, D. A. Beaton, T. Tiedje, A. Chernikov, S. Chatterjee, and M. Koch, J. Appl. Phys. **114**, 164306 (2013).
[10]S. Imhof, C. Wagner, A. Thränhardt, A. Chernikov, M. Koch, N. S. Köster, S. Chatterjee, S. W. Koch, O. Rubel, X. Lu *et al.*, Appl. Phys. Lett. **98**, 161104 (2011).
[11]S. Jin and S. J. Sweeney, J. Appl. Phys. **114**, 213103 (2013).
[12]H. Ben Naceur, T. Mzoughi, I. Moussa, L. Nguyen, A. Rebey, and B. El Jani, Physica E **43**, 106 (2010).
[13]B. N. Zvonkov, I. A. Karpovich, N. V. Baidus, O. Filatov, S. V. Morozov, and Y. Gushina, Nanotechnology **11**, 221 (2000).
[14]P. Ludewig, Z. L. Bushell, L. Nattermann, N. Knaub, W. Stolz, and K. Volz, J. Cryst. Growth **396**, 95 (2014).
[15]P. Ludewig, N. Knaub, W. Stolz, and K. Volz, J. Cryst. Growth **370**, 186 (2013).
[16]N. I. of Standards and Technology, NIST Standard Reference Database Number 20 (visited 2018).
[17]J. Scofield, J. Electron Spectrosc. Relat. Phenom. **8**, 129 (1976).
[18]M. Seah and W. Dench, Surf. Interface Anal. **1**, 2 (1979).
[19]M. Seah and M. T. Anthony, Surf. Interface Anal. **6**, 230 (1984).
[20]M. Seah, M. E. Jones, and M. T. Anthony, Surf. Interface Anal. **6**, 242 (1984).
[21]L. Z. Zhao and J. B. Zhang, Solid State Commun. **90**, 709 (1994).
[22]R. Shimizu, Nucl. Instrum. Methods Phys. Res. **18**, 486 (1986).
[23]Z. L. Liau, B. Y. Tsaur, and J. W. Mayer, J. Vac. Sci. Technol. **16**, 121 (1979).
[24]M. Cardona and P. Y. Yu, *Fundamentals of Semiconductors*, 4th ed. (Springer, 1995), ISBN: 9783642007095.
[25]R. Kubo, J. Phys. Soc. Jpn. **12**, 570 (1957).
[26]G. D. Cody, T. Tiedje, B. Abeles, B. Brooks, and Y. Goldstein, Phys. Rev. Lett. **47**, 1480 (1981).
[27]H. Haug and S. W. Koch, *Quantum Theory of the Optical and Electronic Properties of Semiconductors* (World Scientific, 2003), ISBN: 9788578110796.

BIBLIOGRAPHY

[1] T. Miya et al. “Ultimate low-loss single-mode fibre at 1.55 μm”. In: *Electron. Lett.* 15 (1979), p. 106.

[2] D. O. Caplan. “Laser communication transmitter and receiver design”. In: *J. Opt. Fiber. Commun. Rep.* 4 (2007), p. 225.

[3] A. Vossier, B. Hirsch, and J. M. Gordon. “Is Auger recombination the ultimate performance limiter in concentrator solar cells?” In: *Appl. Phys. Lett.* 97 (2010), p. 193509.

[4] A. R. Beattie and P. T. Landsberg. “Auger effect in semiconductors”. In: *Proc. R. Soc. Lond. A* 249 (1959), p. 16.

[5] S. J. Sweeney and S. R. Jin. “Bismide-nitride alloys: Promising for efficient light emitting devices in the near- and mid-infrared”. In: *J. Appl. Phys.* 113 (2013), p. 043110.

[6] S. Francoeur et al. “Band gap of $GaAs_xBi_{1-x}$, 0<x<3.6%”. In: *Appl. Phys. Lett.* 82 (2003), p. 3874.

[7] S. Tixier et al. “Molecular beam epitaxy growth of $GaAs_{1-x}Bi_x$”. In: *Appl. Phys. Lett.* 82 (2003), p. 2245.

[8] S. J. Sweeney and S. R. Jin. “Contactless electroreflectance study of E_0 and $E_0 + \Delta_{SO}$ transitions in $In_{0.53}Ga_{0.47}Bi_xAs_{1-x}$ alloys”. In: *Appl. Phys. Lett.* 99 (2011), p. 251906.

[9] G. G. Zegrya and A. D. Andreev. “Mechanism of suppression of Auger recombination processes in type-II heterostructures”. In: *Appl. Phys. Lett.* 67 (1996), p. 2681.

[10] J. R. Meyer et al. “Type-II quantum-well lasers for the mid- wavelength infrared”. In: *Appl. Phys. Lett.* 67 (1995), p. 757.

[11] G. G. Zegrya and A. D. Andreev. “Theory of the recombination of nonequilibrium carriers in type-ll heterostructures”. In: *Teor. Fiz.* 109 (1996), p. 615.

[12] S. Gies et al. “Excitonic transitions in highly efficient (GaIn)As/Ga(AsSb) type-II quantum-well structures”. In: *Appl. Phys. Lett.* 107 (2015), p. 182104.

[13] C. A. Broderick et al. “$GaAs_{1-x}Bi_x/GaN_yAs_{1-y}$ type-II quantum wells: novel strain-balanced heterostructures for GaAs-based near- and mid-infrared photonics”. In: *Sci. Rep.* 7 (2017), p. 46371.

[14] L. Vegard. “Die Konstitution der Mischkristalle und die Raumfüllung der Atome”. In: *Z. Physik* 5 (1921), p. 17.

[15] I. Vurgaftman, J. R. Meyer, and L. R. Ram-Mohan. “Band parameters for III–V compound semiconductors and their alloys”. In: *J. Appl. Phys.* 89 (2001), p. 13710.

[16] M. Weyers, M. Sato, and H. Ando. “Red shift of photoluminescence and absorption in dilute GaAsN alloy layers”. In: *JJAP* 31 (1992), pp. L853–L855.

[17] D. J. Friedman et al. “1-eV solar cells with GaInNAs active layer”. In: *J. Cryst. Growth* 195 (1998), pp. 409–415.

[18] W. Shan et al. “Band anticrossing in GaInNAs alloys”. In: *Phys. Rev. Lett.* 82 (1999), p. 1221.

[19] J. D. Perkins et al. “Nitrogen-activated transitions, level repulsion, and band gap reduction in $GaAs_{1-x}N_x$ with $x < 0.03$”. In: *Phys. Rev. Lett.* 82 (1999), p. 3312.

[20] De Gruyter. *IUPAC Standards Online*. visited 2020. URL: https://www.degruyter.com/view/db/iupac.

[21] S. Tiwari and D. J. Frank. “Empirical fit to band discontinuities and barrier heights in III–V alloy systems”. In: *Appl. Phys. Lett.* 60 (1992), p. 630.

[22] K. Alberi et al. “Valence band anticrossing in $GaBi_xAs_{1-x}$”. In: *Appl. Phys. Lett.* 91 (2007), p. 2005.

[23] W. Huang et al. “Molecular-beam epitaxy and characteristics of $GaN_yAs_{1-x-y}Bi_x$”. In: *J. Appl. Phys.* 98 (2005), p. 053505.

[24] J. P. Petropoulos, Y. Zhong, and J. M. O. Zide. "Optical and electrical characterization of InGaBiAs for use as a mid-infrared optoelectronic material". In: *Appl. Phys. Lett.* 99 (2011), p. 031110.

[25] P. Carrier and S. Wei. "Calculated spin-orbit splitting of all diamondlike and zinc-blende semiconductors: Effects of $p_{1/2}$ local orbitals and chemical trends". In: *Phys. Rev. B* 70 (2004), p. 035212.

[26] C. A. Broderick et al. "Band engineering in dilute nitride and bismide semiconductor lasers". In: *Semicond. Sci. Technol.* 27 (2012), p. 094011.

[27] N. Hossain et al. "Improved performance of GaAsSb/GaAs SQW lasers". In: *Novel In-Plane Semiconductor Lasers IX*. Ed. by A. A. Belyanin and P. M. Smowton. International Society for Optics and Photonics. SPIE, 2010, p. 46.

[28] Z. Batool et al. "The electronic band structure of GaBiAs/GaAs layers: Influence of strain and band anti-crossing". In: *J. Appl. Phys.* 111 (2012), p. 113108.

[29] I. P. Marko et al. "Temperature and Bi-concentration dependence of the bandgap and spin-orbit splitting in InGaBiAs/InP semiconductors for mid-infrared applications". In: *Appl. Phys. Lett.* 101 (2012), p. 221108.

[30] L. C. Bannow et al. "Configuration dependence of band-gap narrowing and localization in dilute $GaAs_{1-x}Bi_x$ alloys". In: *Phys. Rev. B* 93 (2016), p. 205202.

[31] J. Hader et al. "Extended band anti-crossing model for dilute bismides". In: *Appl. Phys. Lett.* 112 (2018), p. 062103.

[32] A. Chernikov. "Time-Resolved Photoluminescence Spectroscopy of Semiconductors for Optical Applications Beyond the Visible Spectral Range". PhD thesis. Philipps-Universität Marburg, 2011.

[33] H. Haug and S. W. Koch. *Quantum Theory of the Optical and Electronic Properties of Semiconductors*. World Scientific Publishing, 2003. Chap. Excitons. ISBN: 978-981-3101-11-1.

[34] C. F. Klingshirn. *Semiconductor Optics*. Springer-Verlag Berlin Heidelberg, 1995. Chap. Excitons, Biexcitons, Trions. ISBN: 978-3-642-28361-1.

[35] O. Rubel et al. "Kinetic effects in recombination of optical excitations in disordered quantum heterostructures: Theory and experiment". In: *J. Luminescence* 127 (2007), p. 285.

[36] S. D. Baranovskii, R. Eichmann, and P. Thomas. "Temperature-dependent exciton luminescence in quantum wells by computer simulation". In: *Phys. Rev. B* 58 (1998), p. 13081.

[37] P. Y. Yu and M. Cardona. "Fundamentals of Semiconductors". In: Springer-Verlag Berlin Heidelberg, 1995. Chap. Emission Spectroscopies. ISBN: 978-3-642-00710-1.

[38] B. Batz. "Reflectance modulation at a germanium surface". In: *Solid State Commun.* 4 (1966), p. 241.

[39] D. D. Sell and E. O. Kane. "Piezoreflectance of germanium from 1.9 to 2.8 eV". In: *Phys. Rev.* 185 (1969), p. 1103.

[40] G. Ascarelli. "Experimental Detection of Internal Polaron States Associated with the Indirect Edge of AgBr Using Piezo-Optical Transmission". In: *Phys. Rev. Lett.* 20 (1968), p. 44.

[41] M. Cardona, K. L. Shaklee, and F. H. Pollak. "Electroreflectance at a semiconductor - electrolyte interface". In: *Phys. Rev.* 154 (1967), p. 696.

[42] E. Y. Wang, W. A. Albers, and C. E. Bleil. "Light-modulated Reflectance of Semiconductors". In: *Proceedings of the International Conference on II-VI Semiconducting Compounds, Providence, Rhode Island.* 1967, p. 136.

[43] H. Shen et al. "Dependence of the photoreflectance of semiinsulating GaAs on temperature and pump chopping frequency". In: *Appl. Phys. Lett.* 52 (1988), p. 2058.

[44] D. E. Aspnes. "Third-derivative modulation spectroscopy with low-field electroreflectance". In: *Surface Sci.* 37 (1973), p. 418.

[45] D.E. Aspnes and N. Bottka. "Modulation Techniques". In: Elsevier Ltd., 1972. Chap. Electric-Field Effects on the Dielectric Function of Semiconductors and Insulators, p. 457. ISBN: 978-0-12-752109-1.

[46] P. Y. Yu and M. Cardona. "Fundamentals of Semiconductors". In: Springer-Verlag Berlin Heidelberg, 1995. Chap. Photoemission. ISBN: 978-3-642-00710-1.

[47] National Institute of Standards and Technology. *NIST Standard Reference Database Number 20.* visited 2020. URL: http://dx.doi.org/10.18434/T4T88K.

[48] J. F. Moulder et al. "Handbook of X-ray Photoelectron Spectroscopy". In: Perkin-Elmer Corporation, 1995.

[49] International Organization for Standardization. *Surface chemical analysis — X-ray photoelectron spectrometers — Calibration of energy scales*. visited 2020. URL: https://www.iso.org/standard/55796.html.

[50] M.P. Seah and M. T. Anthony. "Quantitative XPS: The Calibration of Spectrometer Intensity-Energy Response Functions 1". In: *Surf. Interface Anal.* 6 (1984), p. 230.

[51] M.P Seah, M. E. Jones, and M. T. Anthony. "Quantitative XPS: The calibration of Spectrometer Intensity-Energy Response Functions 2". In: *Surf. Interface Anal.* 6 (1984), p. 242.

[52] M.P. Seah and W.A. Dench. "Quantitative Electron Spectroscopy of Surfaces: A Standard Data Base for Electron Inelastic Mean Free Paths in Solids". In: *Surf. Interface Anal.* 1 (1979), p. 2.

[53] J.H. Scofield. "Hartree-Slater subshell photoionization cross-sections at 1254 and 1487 eV". In: *J. Electron Spectrosc.* 8.2 (1976), p. 129.

[54] E. B. Saloman, J. H. Hubbell, and J.H. Scofield. "X-ray attenuation cross sections for energies 100 eV to 100 keV and elements Z = 1 to Z = 92". In: *Atom. Data Nucl. Data* 38 (1988), p. 1.

[55] D. A. Shirley. "High-Resolution X-Ray Photoemission Spectrum of the Valence Bands of Gold". In: *Phys. Rev. B* 5 (1972), p. 4709.

[56] E. B. Saloman, J. H. Hubbell, and J.H. Scofield. "Relative intensities in photoelectron spectroscopy of atoms and molecules". In: *J. Electron Spectrosc.* 8 (1976), p. 389.

[57] H. S. Hansen and S. Tougaard. "Separation of spectral components and depth profiling through inelastic background analysis of XPS spectra with overlapping peaks". In: *Surf. Interface Anal.* 17 (1991), p. 593.

[58] S. Tougaard. "Accuracy of the non-destructive surface nanostructure quantification technique based on analysis of the XPS or AES peak shape". In: *Surf. Interface Anal.* 26 (1998), p. 249.

[59] D. Briggs. "Surface Analysis by Auger and X-ray Photoelectron Spectroscopy". In: IM Publications, 2003. Chap. XPS: Basic Principles, Spectral Features and Qualitative Analysis. ISBN: 978-1-901019-04-9.

[60] J. Schweppe et al. “Accurate measurement of Mg and Al $K_{\alpha 1,2}$ X-ray energy profiles”. In: *J. Electron Spectrosc.* 67 (1994), p. 463.

DANKSAGUNG

Eine wissenschaftliche Arbeit ist nie das Werk einer einzelnen Person, deshalb möchte ich mich an dieser Stelle bei allen Bedanken, die zur Erstellung meiner Arbeit beigetragen haben. Allen voran gilt Sangam Chatterjee als Betreuer meiner Arbeit ein besonderer Dank. Durch seine motivierende Art gelang es ihm, mich für die Spektroskopie und Halbleiterphysik zu begeistern. Außerdem gab er mir während der gesamten Zeit viel Freiraum für eigene Ideen und Projekte, stand aber bei Bedarf immer mit Rat und Tat zur Seite und war somit häufig am Erfolg meiner Machenschaften beteiligt. Vielen Dank für die gute Betreuung und das entgegengebrachte Vertrauen.
Des Weiteren möchte ich mich bei neuen und alten Mitgliedern der Arbeitsgruppe bedanken. Anfangen möchte ich bei Nils Rosemann und Robin Döring, von denen ich nicht nur sehr viel über Spektroskopie gelernt habe, sondern, die mir darüber hinaus auch strukturiertes wissenschaftliches Arbeiten vermitteln konnten. Außerdem sei hier mein Büronachbar Florian Dobener erwähnt, der mir den Arbeitsalltag immer erleichtert hat, immer für Diskussionen jeglicher Natur bereit war und sich zusätzlich durch einen sehr guten Musikgeschmack auszeichnen konnte. Es gelang ihm immer, meine Programmierprobleme - von Quicksort abgesehen - zu lösen. Besonders möchte ich ihm für seinen kritischen Umgang mit Daten und Argumenten bedanken, welche sich auch beim Korrekturlesen meiner Dissertation als nützlich erwies. Seit meinem ersten Semester hat mich Jurek L. als Kommilitone und Freund begleitet, konnte mich immer auf andere Gedanken bringen, aber in den wichtigen Momenten auch stets gut beraten und mir zur Seite stehen. In diesem Sinne: Auf Jurek! Unserem akademischen Oberrat Detlev Hofmann möchte ich für seinen Input und den wissenschaftlichen Austausch danken, insbesondere aber auch für seine Gelassenheit und die Fähigkeit, stres-

sige Situationen gekonnt zu entschärfen. Auch Woldemar Niedenthal soll nicht unerwähnt bleiben, der sich während der Corona-Pandemie unermüdlich und aufopferungsvoll um Essensbestellungen und somit die Versorgung der Arbeitsgruppe gekümmert hat. Auch all den anderen Mitgliedern der AG möchte ich danken, schließlich ist eine angenehme und freundliche Arbeitsatmosphäre der Schlüssel für ein großes Projekt wie diese Dissertation.
Danken möchte ich auch den Personen des I. Physikalischen Instituts für die freundliche und unkomplizierte Aufnahme an der neuen Universität. Insbesondere mit der Unterstützung von Daniela Musaeus und Anja Denhardt konnte ich alle organisatorischen Hindernisse und Formalia bewältigen.
Ein besonderer Dank gilt Thilo Hepp, der sich intensiv mit der Epitaxie und der Strukturanalyse der hier untersuchten Proben beschäftigt hat und seine Kenntnisse immer mit mir geteilt hat. Vielen Dank für die gute und unkomplizierte Zusammenarbeit, für die kurzweilige Gesellschaft auf unseren gemeinsamen Konferenzen sowie das Korrekturlesen dieser Arbeit.
Vielen Dank Kerstin Volz für die Koordination der Epitaxie und Strukturanalyse, aber auch für die Zusammenarbeit sowie die Bereitschaft als Gutachterin dieser Dissertation zu fungieren.
Der Deutschen Forschungsgemeinschaft im Rahmen des *GRK 1782 - Funktionalisierung von Halbleitern* möchte ich für die finanzielle Unterstützung meiner Arbeit danken.
Abschließend möchte ich mich bei Allen bedanken, die mich auf meinem Weg abseits der Promotion begleitet und unterstützt haben. An erster Stelle und besonders möchte ich mich bei meinen Eltern bedanken, die mich immer unterstützt und mir ein Studium überhaupt erst ermöglicht haben. Danke Felix und Andre für die langjährige Freundschaft, die lustigen Abende und die Möglichkeit, einfach Abschalten zu können. Danke Jonathan, für die langen aber dennoch unterhaltsamen Abende im Lernzentrum, die Kickerabende und späten Stunden in der Kneipe, aber im Besonderen für deine Freundschaft, die auch bis nach Bayern reicht. Danke an die Maltes und Julians für die kulturellen Ausflüge und Urlaube nach anstrengenden Semestern. Besonders möchte ich mich bei Laura bedanken. Sie hat nicht nur meine teilweise langen Arbeitszeiten ertragen und war manchmal meinen wechselhaften Launen ausgesetzt, wenn der Arbeitstag nicht so lief, wie ich es mir erhofft hatte, sondern sie hat es immer wieder geschafft, mich aufzubauen, mich zu motivieren und mir ein Lächeln ins Gesicht zu zaubern. Danke für deine Unterstützung!